Springtime high surface ozone events over the western United States: Quantifying the role of stratospheric intrusions

Meiyun Lin,[1,2] Arlene M. Fiore,[3] Owen R. Cooper,[4,5] Larry W. Horowitz,[2] Andrew O. Langford,[5] Hiram Levy II,[2] Bryan J. Johnson,[5] Vaishali Naik,[2,6] Samuel J. Oltmans,[4] and Christoph J. Senff [4,5]

Received 21 May 2012; revised 29 August 2012; accepted 4 September 2012; published 12 October 2012.

[1] The published literature debates the extent to which naturally occurring stratospheric ozone intrusions reach the surface and contribute to exceedances of the U.S. National Ambient Air Quality Standard (NAAQS) for ground-level ozone (75 ppbv implemented in 2008). Analysis of ozonesondes, lidar, and surface measurements over the western U.S. from April to June 2010 show that a global high-resolution ($\sim 50 \times 50$ km^2) chemistry-climate model (GFDL AM3) captures the observed layered features and sharp ozone gradients of deep stratospheric intrusions, representing a major improvement over previous chemical transport models. Thirteen intrusions enhanced total daily maximum 8-h average (MDA8) ozone to ~70–86 ppbv at surface sites. With a stratospheric ozone tracer defined relative to a dynamically varying tropopause, we find that stratospheric intrusions can episodically increase surface MDA8 ozone by 20–40 ppbv (all model estimates are bias corrected), including on days when observed ozone exceeds the NAAQS threshold. These stratospheric intrusions elevated background ozone concentrations (estimated by turning off North American anthropogenic emissions in the model) to MDA8 values of 60–75 ppbv. At high-elevation western U.S. sites, the 25th–75th percentile of the stratospheric contribution is 15–25 ppbv when observed MDA8 ozone is 60–70 ppbv, and increases to ~17–40 ppbv for the 70–85 ppbv range. These estimates, up to 2–3 times greater than previously reported, indicate a major role for stratospheric intrusions in contributing to springtime high-O_3 events over the high-altitude western U.S., posing a challenge for staying below the ozone NAAQS threshold, particularly if a value in the 60–70 ppbv range were to be adopted.

Citation: Lin, M., A. M. Fiore, O. R. Cooper, L. W. Horowitz, A. O. Langford, H. Levy II, B. J. Johnson, V. Naik, S. J. Oltmans, and C. J. Senff (2012), Springtime high surface ozone events over the western United States: Quantifying the role of stratospheric intrusions, *J. Geophys. Res.*, *117*, D00V22, doi:10.1029/2012JD018151.

1. Introduction

[2] Understanding global sources of local air pollution is crucial for setting air quality standards and for designing appropriate control policies [*National Research Council*, 2009; *McDonald-Buller et al.*, 2011]. In contrast to the "good" ozone (O_3) layer in the stratosphere that shields life on Earth from the Sun's harmful ultraviolet radiation, exposure to high concentrations of ground-level (i.e., "bad") O_3 aggravates respiratory illness [*World Health Organization*, 2005] and damages vegetation. Stratosphere-to-troposphere transport (STT) is a common occurrence at mid- and high latitudes, but its influence on tropospheric O_3 levels remains a long-standing question despite decades of research [*Levy et al.*, 1985; *Roelofs and Lelieveld*, 1997; *Monks*, 2000; *Stohl et al.*, 2003; *Stevenson et al.*, 2006; *Wild et al.*, 2007; *Hsu and Prather*, 2009]. In particular, prior publications debate the extent to which stratospheric O_3 intrusions reach the surface [*Oltmans and Levy*, 1992; *Moody et al.*, 1995; *Li et al.*, 2002; *Ding and Wang*, 2006] and increase U.S. ground-level O_3 over the health-based limit [*Lefohn et al.*, 2001, 2011; *Fiore et al.*, 2003; *Langford et al.*, 2009]. This poor understanding reflects our inability to directly measure

[1]Atmospheric and Oceanic Sciences, Princeton University, Princeton, New Jersey, USA.
[2]Geophysical Fluid Dynamics Laboratory, NOAA, Princeton, New Jersey, USA.
[3]Department of Earth and Environmental Sciences and Lamont-Doherty Earth Observatory, Columbia University, Palisades, New York, USA.
[4]Cooperative Institute for Research in Environmental Sciences, University of Colorado Boulder, Boulder, Colorado, USA.
[5]NOAA Earth System Research Laboratory, Boulder, Colorado, USA.
[6]University Corporation of Atmospheric Research, Boulder, Colorado, USA.

Corresponding author: M. Lin, Atmospheric and Oceanic Sciences, Princeton University, 201 Forrestal Rd., Princeton, NJ 08540, USA. (meiyunl@princeton.edu)

©2012. American Geophysical Union. All Rights Reserved.
0148-0227/12/2012JD018151

the stratospheric contribution to tropospheric O_3, as well as limited model capability to represent the dynamic processes of STT and to account accurately for stratospheric O_3 in the troposphere [e.g., *Roelofs et al.*, 2003; *Hudman et al.*, 2004; *Hsu et al.*, 2005; *Hess and Lamarque*, 2007; *Zhang et al.*, 2011]. Here we revisit the role of stratospheric influence on springtime high surface O_3 episodes over the western United States by applying a newly developed global model with fully coupled stratosphere-troposphere chemistry at $\sim 50 \times 50$ km^2 resolution (GFDL AM3) [*Lin et al.*, 2012], which we analyze alongside a suite of satellite and in situ measurements.

[3] The primary mechanism for the transport of stratospheric O_3 to the mid- and lower troposphere is descent through the dry airstream of midlatitude cyclones [*Danielsen*, 1968; *Johnson and Viezee*, 1981; *Cooper et al.*, 2001; *Stohl et al.*, 2003]. Western North America, located at the end of the North Pacific midlatitude storm track, has been identified as a preferred region for deep STT reaching below the 700 hPa level [*Sprenger and Wernli*, 2003; *James et al.*, 2003]. The semi-permanent surface anticyclone in the eastern North Pacific Ocean provides a baroclinic zone that facilitates descent of stratospheric O_3 into the lower troposphere following strong frontal passages [*Bourqui and Trepanier*, 2010]. The impacts of deep STT events on surface O_3 are strongest at Northern Hemisphere extratropical latitudes in late winter and spring, likely reflecting a combination of peak O_3 abundances at the tropopause [e.g., *Prather et al.*, 2011], more frequent storms [e.g., *Holton et al.*, 1995] and a longer O_3 lifetime than in summer, and stronger surface heating that enhances the turbulent mixing between the free troposphere (FT) and the planetary boundary layer (PBL) compared to early winter.

[4] Signatures of stratospheric intrusions in the FT have been observed in various contexts. For example, they appear as filamentary dry features in satellite water vapor imagery [e.g., *Appenzeller and Davies*, 1992; *Wimmers et al.*, 2003; *Felker et al.*, 2011] and as layered structures in O_3 profiles [e.g., *Oltmans et al.*, 1996; *Roelofs et al.*, 2003; *Thompson et al.*, 2007]. They are evident in ozone lidar measurements [e.g., *Browell et al.*, 1987; *Langford et al.*, 1996; *Stohl and Trickl*, 1999], and have long been detected by in situ aircraft measurements [*Danielsen*, 1968; *Shapiro*, 1980; *Cooper et al.*, 2004, 2005; *Bowman et al.*, 2007] and by using meteorological tracers like PV and chemical tracers like ^{7}Be [*Danielsen et al.*, 1987; *Stohl et al.*, 2003].

[5] Despite observational evidence for the presence of stratospheric intrusions in the FT, accurately quantifying the stratospheric contribution to tropospheric O_3 in space and time is complicated by the interplay of processes influencing O_3 from STT (e.g., circulation and abundances of O_3 in the lower stratosphere; an ever shifting, folding tropopause; filamentary intrusions; evolution in transit due to chemical and depositional losses, and dilution). Many global and regional tropospheric chemical transport models (CTMs) do not reproduce well the layered features of stratospheric intrusions measured by ozonesondes and lidar [e.g., *Roelofs et al.*, 2003; *Hudman et al.*, 2004; *Liang et al.*, 2007; *Tarasick et al.*, 2007]. Modeling the impacts of STT in surface air is further complicated by model limitation in representing meso-scale dynamics, e.g., nocturnal low-level jets and mountain-driven lee wave breaking [*Johnson and Viezee*, 1981], which influence the amount of O_3 entrained into the PBL.

[6] The current guidelines from the U.S. Environmental Protection Agency (EPA) state that air quality monitoring data influenced by an extreme stratospheric O_3 intrusion may be excluded from regulatory determinations related to violations of the U.S. National Ambient Air Quality Standard (NAAQS) for ground-level O_3, since these naturally occurring "exceptional events" are not reasonably controllable by state agencies [*U.S. Environmental Protection Agency* (*U.S. EPA*), 2007]. The states in the U.S. EPA Region 8 (Figure 1) are particularly susceptible to these events [*State of Colorado*, 2011; *State of Wyoming*, 2011]. The identification of such events is challenging, however, given the episodic, transient and localized nature of deep STT and the limited spatial and temporal extent of measurements available to diagnose their presence as well as potential coincident O_3 photochemical production from local emissions. Historically, the U.S. EPA has relied heavily on the GEOS-Chem global CTM for estimating background O_3 for policy assessments [e.g., *Fiore et al.*, 2002, 2003; *U.S. EPA*, 2006; *Zhang et al.*, 2011], however, studies have shown that GEOS-Chem underestimates the contribution from deep STT events to lower tropospheric O_3 [*Hudman et al.*, 2004] and is unable to capture observed O_3 above 70 ppbv at remote mountain sites in spring [*Emery et al.*, 2012; *Zhang et al.*, 2011], which may reflect stratospheric influence.

[7] For the first time, we apply a global high-resolution ($\sim 50 \times 50$ km^2) chemistry-climate model [*Lin et al.*, 2012], with a stratospheric O_3 tracer defined relative to a dynamically varying tropopause tracer recently proposed by *Prather et al.* [2011], to quantify stratospheric impacts on surface O_3 episodes over the western U.S. Our focus on the western U. S. leverages the availability of near-daily ozonesonde and lidar measurements during the 2010 NOAA CalNex field campaign in California [*Cooper et al.*, 2011; *Langford et al.*, 2012], which allows for an unprecedented opportunity to evaluate GFDL AM3 on a process level, in particular, its representation of the dynamic processes conducive to surface impacts from stratospheric intrusions.

[8] Section 2 briefly describes the measurements, model simulations, and stratospheric O_3 tagging methodology. Section 3 presents several case studies of the strongest and deepest STT events in April–June 2010, using both the model and observations to assess stratospheric influence on the NAAQS exceedances. Section 4 summarizes the ability of the GFDL AM3 model to represent the relevant processes. We then synthesize mean and maximum stratospheric contributions to O_3 levels at more than 1200 surface monitoring sites and discuss associated policy implications (Section 5).

2. Measurements and Model

2.1. Upper Air and Surface Measurements

[9] We use a combination of water vapor images from the NOAA GOES-West geostationary satellite, total column O_3 retrieved from the Atmospheric Infrared Sounder (AIRS) onboard the NASA Aqua satellite [*Susskind et al.*, 2003], and NCEP Global Forecasting System Final Analysis (FNL) to provide a large-scale view of observed synoptic conditions favorable for stratospheric intrusions. The GOES water vapor images used here indicate upper-tropospheric relative

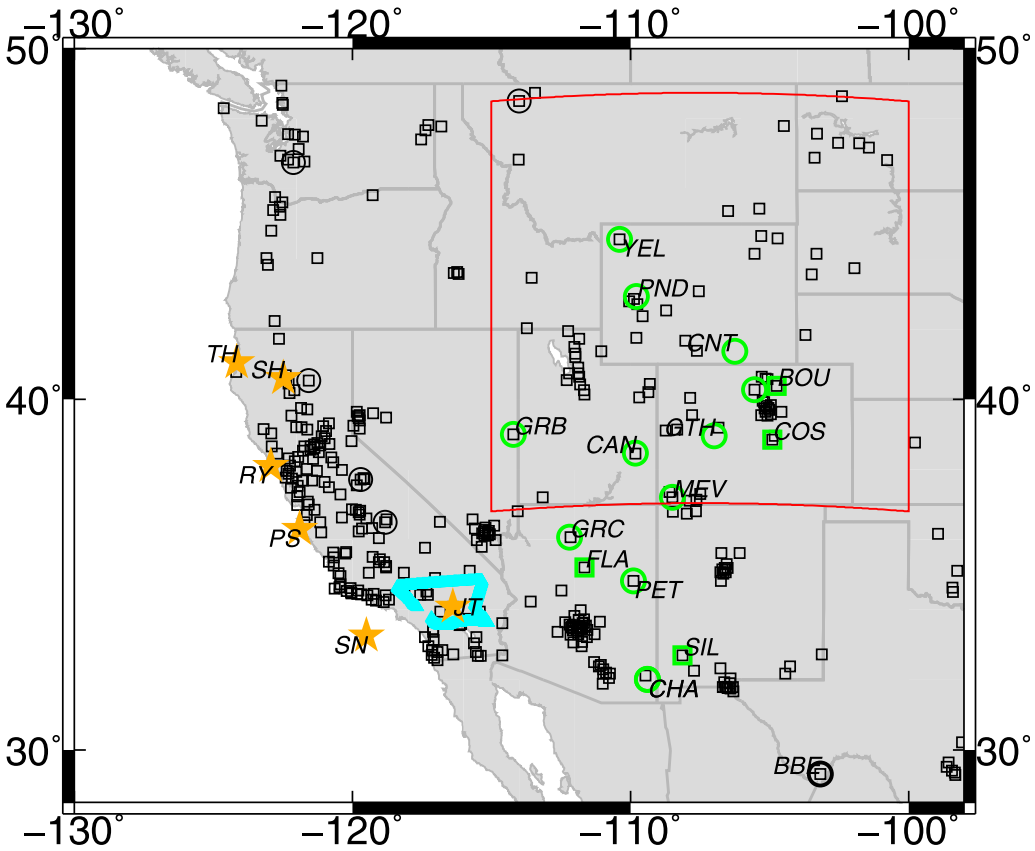

Figure 1. Map showing locations of six ozonesonde sites (orange stars) in California, flight path of an aircraft-based ozone lidar on May 23 (solid cyan, Figure 7), and surface monitoring sites from CASTNet (circles) and AQS (squares). The green symbols indicate 15 select sites analyzed in 12b. The red box encloses the AQS sites analyzed in Figure 12a. These AQS sites are primarily located in EPA Region 8 (Utah, Colorado, Wyoming, Montana, North and South Dakota).

humidity (RH), thus they convolve humidity with temperature and will be too moist in cold regions, while too dry in warm regions as discussed by *Wimmers and Moody* [2001]. There are similar issues for the RH values from the radiosondes, which we use to identify the dry layers as a qualitative proxy for air of stratospheric origin.

[10] We gain insights into the deep descent of stratospheric O_3 from near-daily balloon-borne ozonesondes launched at six sites in California (Figure 1) between May 10 and June 19, 2010 [*Cooper et al.*, 2011]. Three of the sonde launch sites were located on the California coast from north to south: Trinidad Head (TH), Point Reyes (RY), and Point Sur (PS). One site, Shasta (SH), was located in the Northern Sacramento Valley. There were also two sites in Southern California: San Nicholas Island (SN), ~140 km southwest of Los Angeles, and Joshua Tree (JT), located in the Mojave Desert on the northwest edge of Joshua Tree National Park. For comparison with ozonesonde measurements, we sample AM3 at the locations and times of sonde launches as described by *Lin et al.* [2012]. The O_3 distribution in the lower troposphere was also measured by a downward looking lidar on the NOAA Twin Otter aircraft during two intrusions (May 23 and 29) over Southern California [*Alvarez et al.*, 2011; *Langford et al.*, 2012]. We average the lidar measurements over a 0.5° × 0.625° grid for direct comparison to the AM3 results sampled along the flight track.

[11] Finally, we investigate ground-based measurements of O_3 and meteorological parameters from the U.S. EPA's Clean Air Status and Trends Network (CASTNet), with sites mostly located in rural areas, and from the Air Quality System (AQS), with sites predominantly clustered in urban areas, for changes of surface O_3 levels following the appearance of enhanced O_3 in the FT observed by sondes or lidar. Fifteen high-elevation (>1.4 km above mean sea level, a.s.l.) CASTNet and AQS sites (green symbols in Figure 1) are selected to represent general patterns of stratospheric influence in the mountainous regions. We focus our analysis on daily maximum 8-h average O_3 (hereafter MDA8 O_3), which usually includes the afternoon hours when the boundary layer is sufficiently deep to mix O_3 aloft down to the surface.

2.2. GFDL AM3 Model Simulations

[12] We have recently applied a new version of GFDL AM3 chemistry-climate model at C180 cubed-sphere grid resolution of ~50 × 50 km^2, nudged to GFS winds, to study transport of Asian O_3 pollution to the western U.S. surface during CalNex [*Lin et al.*, 2012]. In order to minimize the impacts of noise near the tropopause introduced via nudging, which has been shown to lead to excessive O_3 STT [e.g., *van Noije et al.*, 2004], we weaken the nudging strength with

decreasing pressure as described by *Lin et al.* [2012]. The global net stratosphere-to-troposphere flux of O_3, diagnosed as the net change due to advection in each grid cell up to the e90 tropopause (Section 2.3) archived from the model every 3 h, is ~535 Tg/yr in nudged AM3, within the observation-based range of 400–600 Tg/yr [e.g., *McLinden et al.*, 2000; *Hsu et al.*, 2005].

[13] AM3 employs the PBL scheme of *Lock et al.* [2000], including a representation of nonlocal mixing in unstable layers and an explicit entrainment parameterization. A recent evaluation shows that AM3 reproduces observed spatial, seasonal and diurnal variability of PBL heights over the U.S. but tends to overestimate shallow, stable nighttime and winter PBL heights [*Seidel et al.*, 2012]. Comparison of the diurnal and day-to-day variability of AM3 surface O_3 between the free running climate model and the nudged version suggests that nudging does not introduce abnormal transport from the FT to the PBL.

[14] A detailed description of model initialization is provided in *Lin et al.* [2012]. Major AM3 model updates since then include: (1) implementing the Fast-JX photolysis scheme [*Wild et al.*, 2000] coupled to cloud and aerosol properties in the AM3 radiation scheme (J. Liu, personal communication, 2011), and (2) using global anthropogenic emissions from RCP8.5 for 2010 [*Moss et al.*, 2010] to better represent recent emission changes in Asia, North America, and Europe. We find that NO_x emissions in RCP8.5 for 2010 are approximately 35% lower over heavily populated regions than those in the U.S. National Emission Inventory (NEI) for 2005, consistent with changes in the 2005–2010 satellite measurements of NO_2 columns from the SCIAMACHY sensor (data available on www.tenis.nl).

[15] In addition to the standard simulation, we conducted a sensitivity simulation with North American (NA; 15°N-90°N, 165°W-60°W) anthropogenic emissions switched off in the model to estimate background O_3 levels, defined by U.S. EPA as O_3 concentrations that would exist in the absence of anthropogenic emissions from U.S., Canada, and Mexico (previously referred to as policy relevant background O_3 [*McDonald-Buller et al.*, 2011]; hereafter NA background). The specific sources of the NA background include STT, intercontinental transport (e.g., Asian pollution), and O_3 produced by wildfire and biogenic emissions, methane, and lightning NO_x.

[16] Accurate representation of O_3 levels in a stratospheric intrusion depends strongly on O_3 simulated in the lower stratosphere [*Roelofs et al.*, 2003; *Terao et al.*, 2008]. AM3 includes fully coupled stratosphere-troposphere-aerosol chemistry within a general circulation model [*Donner et al.*, 2011], with 48 vertical levels, ranging in thickness from 70 m near the Earth's surface to 1–1.5 km near the tropopause and 2–3 km in much of the stratosphere. Observed sea surface temperatures and sea ice, well mixed greenhouse gas and halogen concentrations, and optical properties of stratospheric aerosols are specified in AM3 as time-varying fields. The major stratospheric O_3 destruction cycles (O_x, HO_x, NO_x, ClO_x, and BrO_x) are included explicitly in the model, as well as heterogeneous reactions on ice and nitric acid trihydrate (NAT) in polar stratospheric clouds (PSCs) *[Austin and Wilson*, 2006, 2010]. The fully coupled tropospheric and stratospheric chemistry described more fully in V. Naik et al. (Preindustrial to present day impact of changes in short-lived pollutant emissions on atmospheric composition and climate forcing, submitted to *Journal of Geophysical Research*, 2012) distinguishes the GFDL AM3 model from most current generation global tropospheric CTMs, which represent stratospheric O_3 distributions with simplified stratospheric chemistry (SYNOZ or LINOZ) or by relaxing to an observed climatology [*McLinden et al.*, 2000; *Horowitz et al.*, 2003; *Fiore et al.*, 2003; *Emmons et al.*, 2010; *Zhang et al.*, 2011].

2.3. Quantifying Stratospheric Contributions to Troposphere Ozone

[17] The AM3 simulation of O_3 from STT is entirely driven by winds, with no dependency on the definition of tropopause. Here we implement the dynamically varying e90 tropopause tracer proposed by *Prather et al.* [2011] to tag O_3 originating from the stratosphere (O_3S). Thus, only the O_3S tracer used to account for the STT contribution to tropospheric O_3 (not the full-chemistry O_3 simulation itself) relies on the e90 tropopause definition.

[18] With a globally uniform surface source and 90-day e-folding lifetime, the e90 tracer differentiates tropospheric air by time scales, linking it to the mixing of the troposphere and its exchange with the surface. The e90 tracer approach allows for clear characterization of stratospheric versus tropospheric air in complex situations where the traditional tropopause definitions (e.g., thermal lapse rate, PV, or O_3) are problematic. The tropopause value of e90 is derived as 85 ppbv in AM3 from the constraint that the troposphere annually comprises about 80% of the atmosphere [*Prather et al.*, 2001, 2011]. Monthly mean e90-tropopause pressures and O_3 concentrations in AM3 reproduce the salient features of a climatology derived from ozonesondes (not shown).

[19] We set the O_3S tracer equal to simulated O_3 in stratospheric air (e90 < 85 ppbv) and subject it to chemical loss in tropospheric air (e90 > = 85 ppbv) and depositional loss to the surface in the same manner as O_3 in the troposphere. Aged tropospheric air occasionally includes e90 < 90 ppbv below 600 hPa in the tropics [*Prather et al.*, 2011; M. Prather, personal communication, 2011], so we restrict tagging O_3S to above 600 hPa. Ozone in the stratosphere has been spun up for decades. The O_3S and e90 tracers have been spun up for three years in a previous simulation.

[20] This stratospheric O_3 tagging methodology has a number of mechanistic and conceptual advantages over the methods used in prior publications. The e90 methodology is less prone to errors associated with defining the tropopause in complex synoptic conditions (e.g., midlatitude frontal zones), as compared to using a tropopause fixed at the 100 hPa level [*Roelofs and Lelieveld*, 1997; *Lelieveld and Dentener*, 2000] or defined by the 2 K km^{-1} thermal lapse rate [e.g., *Emmons et al.*, 2003; *Lamarque and Hess*, 2004; *Lin et al.*, 2012]. In the latter methods, any O_3 above the "tropopause" is instantly labeled as "stratospheric" regardless of its true origin. We find that the lapse-rate tagging method overestimates O_3S in surface air by 5–8 ppbv (seasonal average) as compared to the e90 tagging, and occasionally by ~30 ppbv during events when e90 indicates an influence of tropospheric background rather than a stratospheric intrusion (not shown). The estimates of stratospheric

Table 1. Stratospheric Ozone Intrusion Events Over the Western U.S. From April–June 2010[a]

Events	Synoptic Conditions in Satellite Imagery	Descent Captured in Ozonesondes/Lidar	Major Surface Impact Regions[b]	Peak MDA8 O_3 (ppbv)	Number of Exceedances
Apr. 7	AIRS	Not measured	Colorado, New Mexico (Figure 9)	71	-
Apr. 9	AIRS	Not measured	Wyoming (Figure 9)	75	1
Apr. 12–15	**AIRS (Figure S1)**	**Not measured**	**Four Corners Region (Figure 8)**	**86**	**13**
Apr. 21–23	AIRS	Not measured	Colorado, New Mexico (Figure 9)	72	-
Apr. 28–29	AIRS	Not measured	Colorado, Wyoming (Figure 9)	69	-
May 11–13	AIRS/GOES	*Langford et al.* [2012]	Arizona, New Mexico, W. Texas (Figure 9)	74	-
May 18–21	AIRS [*Lin et al.*, 2012]	*Lin et al.* [2012]	Wyoming (Figure 9)	74	-
May 22–24	**AIRS/GOES (Figure S2)**	**Figures 7 and S3**	**Colorado, New Mexico (Figures 8 and 10)**	**79**	**4**
May 27–29	**AIRS/GOES (Figure S4)**	**Figure 5**	**Arizona, California, Colorado (Figures 6 and 10)**	**82**	**5**
Jun. 7–8	**AIRS/GOES (Figure 2)**	**Figure 3**	**Idaho, Utah, Wyoming (Figure 4)**	**76**	**3**
Jun. 9–14	**AIRS/GOES (Figure 2)**	**Figure 3**	**California, Utah, Spread in Southwest (Figure 4)**	**73**	**-**
Jun. 16–17	AIRS/GOES	*Lin et al.* [2012]	Colorado (Figure 9)	67	-
Jun. 22–23	AIRS	Not measured	Colorado (Figures 9 and 10)	77	1

[a]Boldfacing denotes case studies in Sections 3.2–3.4.
[b]A list of affected surface sites in the AQS and CASTNet networks is provided in auxiliary Table S1.

influence for deep intrusions are less sensitive to the O_3S tagging method used.

[21] The dynamical coupling of stratospheric chemistry and transport with the troposphere in AM3, as opposed to imposing a climatological STT O_3 source in previous models [e.g., *Fiore et al.*, 2003; *Zhang et al.*, 2011], allows AM3 O_3S to better capture the dynamic variability of mid- and upper tropospheric O_3 due to stratospheric influence. The O_3S-e90 tagging method also avoids potential noise that may bias the NO_x tagging technique in which the stratospheric contribution is determined as the residual between two much larger numbers [*Hess and Lamarque*, 2007; *Pfister et al.*, 2008]. The new O_3S tracer, implemented in a full-chemistry model like GFDL AM3, accounts for long-range transport and chemical losses of transported stratospheric O_3 in tropospheric air as compared to a tracer in a passive trajectory model like FLEXPART [e.g., *Cooper et al.*, 2005; *Langford et al.*, 2012].

3. Contribution of Deep Stratospheric Intrusions to Surface Ozone Episodes

3.1. April–June 2010: An Active Period for Deep Intrusions

[22] Spring 2010 was unusually cool along the U.S. West Coast with strong surface cold fronts and amplified upper level troughs. The mass of O_3 in the 7–10 km range at Trinidad Head sonde was 39% above the 2004–2009 average [*Cooper et al.*, 2011]. According to the NOAA Climate Prediction Center (http://www.cpc.ncep.noaa.gov), the 2009–2010 winter was influenced by strong El Niño conditions. Several studies have suggested enhanced STT in winter and spring over western North America following El Niño conditions [*Langford et al.*, 1998; *Koumoutsaris et al.*, 2008].

[23] Thirteen stratospheric O_3 intrusions occurred in April–June 2010 (Table 1). Seven events were measured by in situ and remote sensing instruments deployed during the CalNex field campaign from May 9–June 20. Two of these intrusions (May 17–20 and June 16–19) were mixed with Asian pollution [*Lin et al.*, 2012]. *Langford et al.* [2012] used principal component analysis (PCA) of O_3 measurements together with meteorological parameters to infer that these intrusions can account for ~13% of surface O_3 variability in the Los Angeles area during CalNex. Here we further explore five of the strongest intrusions (June 7–8, June 9–14, May 27–29, May 22–24, and April 12–14) in Sections 3.2–3.4 and quantify their impacts on western U.S. surface O_3. Section 3.5 summarizes the influence of all thirteen events on the day-to-day variability of surface O_3 from April–June 2010.

3.2. Dynamic Processes Conducive to Surface Impacts: June 7–14 Intrusions

[24] We examine in this section the dominant meteorological conditions favorable for the direct transport of stratospheric O_3 to the surface of the Northwest versus the Southwest U.S., as illustrated by the June 7–14 intrusions.

[25] Figure 2 depicts the development and intensification of two southeastward penetrating upper-level troughs during June 7–12 and their impacts on the downward transport of stratospheric O_3 to the lower troposphere. On June 7, the dry airstream of a midlatitude cyclone was advected southeastward toward the northwest U.S. (Figure 2a), visible as the dry feature (green and blue) in the water vapor image (Figure 2d). A latitude-height curtain plot of O_3 distributions in AM3 reveals that O_3 from a tropopause fold descended isentropically toward the south to as low as 1 km above the surface off the coast of Los Angeles (Figure 2g). The June 7 and 8 soundings launched along the California coast recorded approximately 80 ppbv of O_3 and RH below 5% at 1.0–3.5 km a.s.l. (Figure 3, first row). These features strongly support the AM3 attribution of a sharp layer of enhanced O_3 above the boundary layer to stratospheric origin. On June 8, MDA8 O_3 values of 70–76 ppbv were detected at ~20 surface sites in Idaho, Utah and Wyoming (Figure 4 (top) and auxiliary material Table S1).[1] Coincident meteorological measurements at the CASTNet sites suggest that these O_3 enhancements were associated with dry and cold conditions (not shown). AM3 consistently estimates 20–35 ppbv of stratospheric contribution in these locations, although it slightly displaces the peak levels in surface air to the northwest.

[26] Between June 9 and 10, a new upper-level trough formed and propagated southeastward to Northern Nevada (Figures 2b, 2e, and 2h). The June 9–10 soundings over Shasta, located on the western edge of the trough, measured >150 ppbv of O_3 within the tropopause fold at 9 km a.s.l.,

[1]Auxiliary materials are available in the HTML. doi:10.1029/2012JD018151.

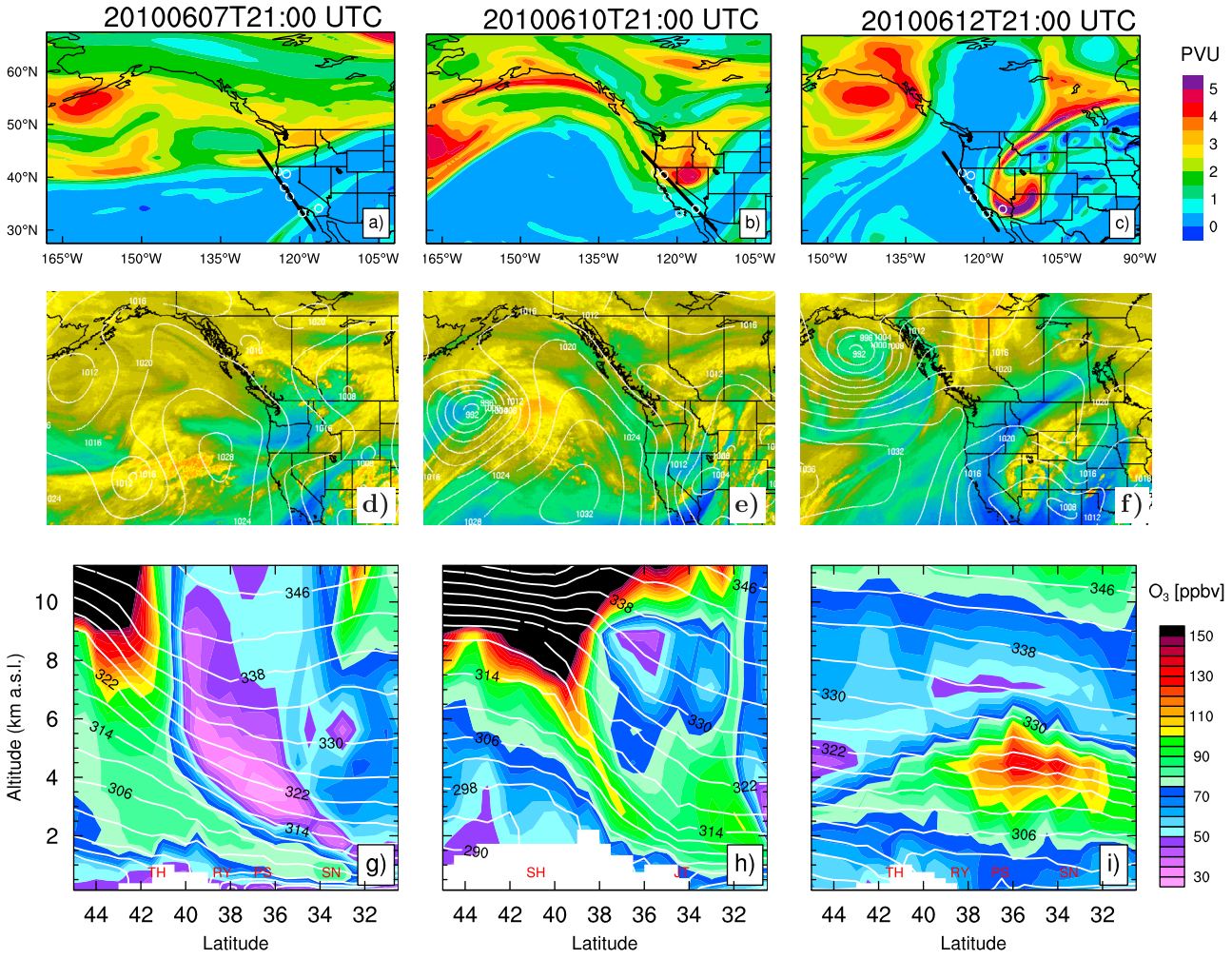

Figure 2. Synoptic conditions during June 7–14 intrusions: (a–c) AM3 250 hPa potential vorticity; (d–f) GOES water vapor images (with mean sea level pressure contours), which indicates relative humidity in the mid- to upper troposphere (Section 2.1), with reds and yellows indicating moist air and blues and greens indicating drier air; (g–i) latitude-height curtain plots of AM3 O_3 distributions (shading) and isentropic surfaces (contoured in K) along the coastal or inland transects (thick lines) in Figures 2a–2c. White circles in Figures 2a–2c and red letters in Figures 2 g–2i denote locations of ozonesondes.

while both the Point Reyes and Point Sur sondes measured stratospheric O_3 remnants at 2–6 km a.s.l. (Figure 3, second and third rows). By June 10, observed O_3 at Joshua Tree increased by a factor of 4 between 4 and 6 km from the previous day, indicating the arrival of stratospheric air to the lower troposphere of Southern California. At the surface downwind of the trough (Figure 4, second row), the Nevada Great Basin and California Mojave Desert experienced elevated O_3 with stratospheric O_3 contributing as much as ~50% of the total in the model.

[27] By June 12, this intrusion evolved into an elongated (~2000 km) and slender (~200 km) streamer, which is visible in the GOES water vapor image (Figure 2f) and represented in AM3 as greater than 4–5 PVU of potential vorticity at 250 hPa (Figure 2c). The development of a cut-off low and tropopause folding led to the formation of a distinct O_3 layer between 3 and 6 km above California in the model (Figure 2i), in remarkable agreement with an O_3 maximum in very dry air measured by the June 12 soundings (Figure 3, fourth row). The Joshua Tree sounding shows an interleaved structure of stratospheric (dry, O_3-enriched) and tropospheric (moist, O_3-depleted) air consistent with a typical cut-off low feature [*Price and Vaughan*, 1993; *Cooper et al.*, 1998]. The tropopause at Joshua Tree is substantially lower on June 12 compared with the previous days.

[28] Injected stratospheric O_3 from this cut-off low was transported into surface air over the Southwest between June 12 and 15 (Figure 4, third and fourth rows). The PCA of *Langford et al.* [2012] shows a corresponding peak in the stratospheric contribution to surface air in the Los Angeles Basin on June 12. Transported stratospheric O_3 enhanced MDA8 O_3 above 70 ppbv at surface monitoring sites as far south as the U.S. Mexico border on June 14 (not shown). By June 15, widespread entrainment of stratospheric O_3 into the boundary layer contributed 30–40 ppbv to MDA8 O_3, and when combined with locally produced O_3 led to MDA8 O_3 levels in excess of 60 ppbv over the entire Southwest region.

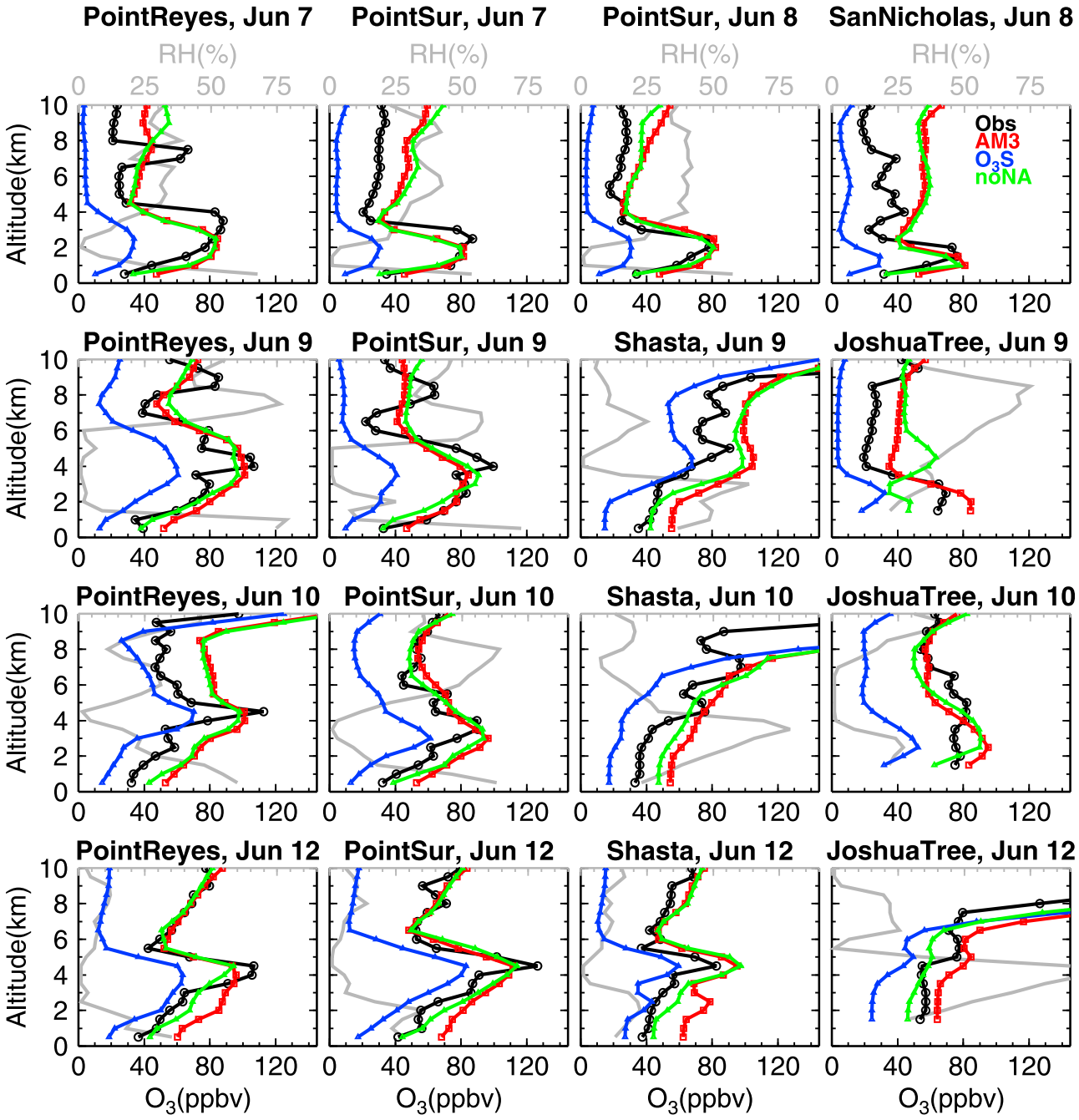

Figure 3. Ozone profiles at the June 7–12 soundings as observed (black) and estimated (red) by the GFDL AM3 model. Also shown are observed relative humidity (gray), AM3 stratospheric O_3 tracer (blue) (Section 2.3), and estimated O_3 with North American anthropogenic emissions turned off (green) (Section 2.2). Model results have been interpolated to sonde pressure and averaged over 0.5-km altitude bins. San Nicholas RH values measured by an unreliable radiosonde are not shown.

[29] The dynamic processes discussed above indicate an important role of deep stratospheric intrusions in driving the regional variability of surface O_3 over the western U.S. (e.g., Figure 4). Stratospheric intrusions that remain close to the polar jet stream above Southern Canada and the Northern U.S. primarily affect the surface of Wyoming, Utah and Colorado located immediately in the southern flank of the polar jet (e.g., June 7–8). In contrast, intrusions that break away from the polar jet as they advect toward the south are more effective at transporting O_3 to the lower troposphere of the Southwest and into surface air over regions within California, Arizona and New Mexico (e.g., June 9–14).

3.3. Stratospheric Influence on a Polluted Region: The May 27–29 Intrusion

[30] A qualitatively similar meteorological situation occurred on May 27–29 (Figure S4 in auxiliary material Text S1). This intrusion appeared as a filamentary feature

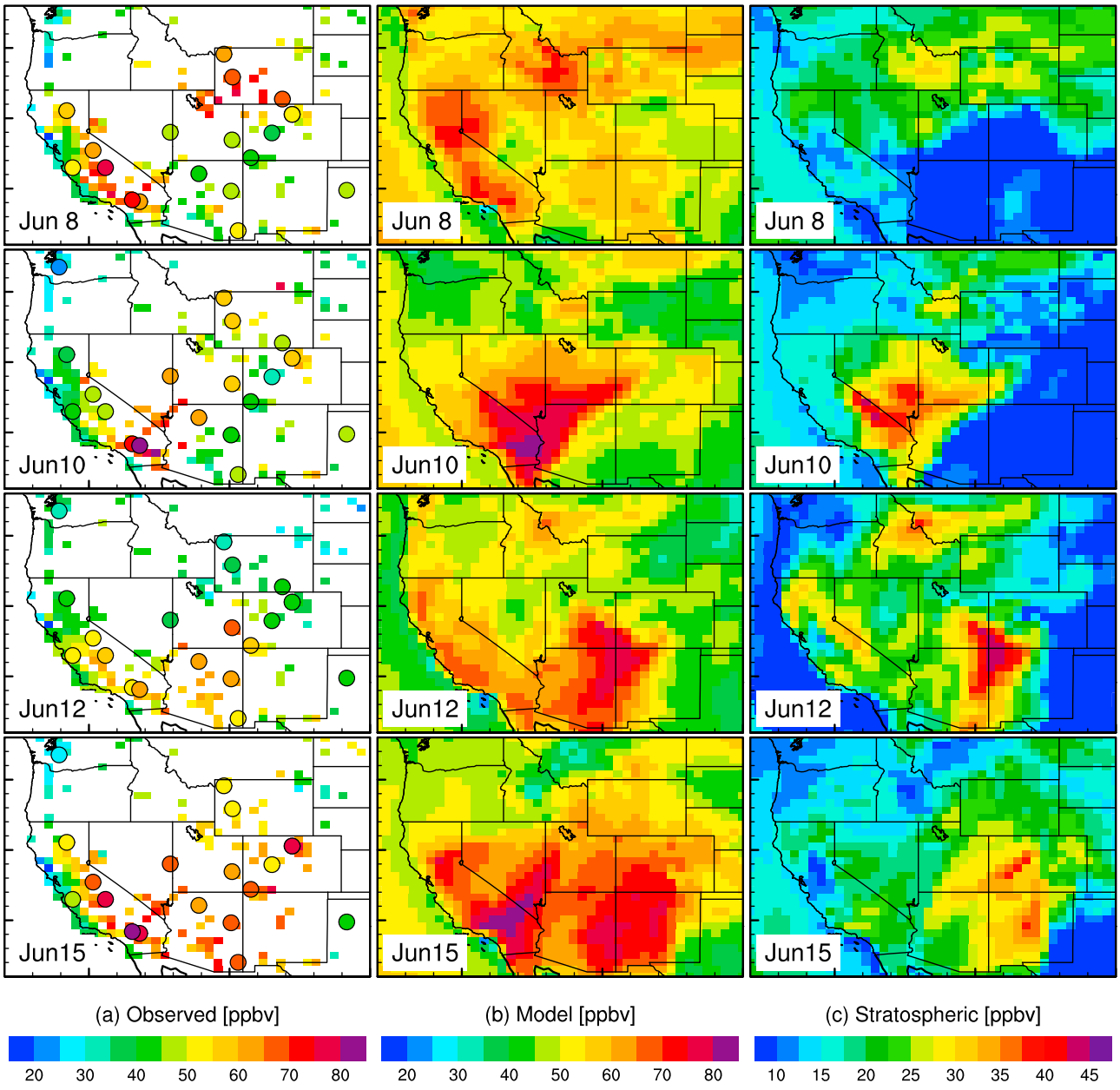

Figure 4. Daily maximum 8-h average O_3 in surface air from June 8–15: (a) observed at CASTNet sites (circles) and AQS (squares) on the same 0.625° by 0.5° grid for AM3, (b) simulated by the GFDL AM3 model and (c) the stratospheric contribution (on a different color scale).

extending from the Gulf of Alaska to the California coast on May 27. A strong surface anticyclone developed over the eastern North Pacific Ocean on May 28, facilitating more effective transport of stratospheric O_3 to the lower troposphere of Southern California during this intrusion as compared to other events.

[31] The May 28 soundings measured an approximately 2-km thick layer of elevated O_3 in excess of 100–150 ppbv sloping from 5 to 7 km above Northern California (Point Reyes and Shasta) to 2–4 km above Southern California (Joshua Tree and San Nicholas), coincident with decreasing RH, a marker for air of stratospheric origin (Figure 5). The elevated-O_3 layer just 2 km above Joshua Tree National Park persisted from May 28 through May 29, when it was also measured by an aircraft-based lidar [*Langford et al.*, 2012]. AM3 captures these narrow layers of enhanced O_3 and estimates a stratospheric contribution of approximately 75%.

[32] Given that San Nicholas Island and Joshua Tree National Park are each located just ~150 km away from the densely populated Los Angeles Basin, locally produced pollution may impact the lower FT of this region under favorable meteorological conditions. Here we find in the model that simulated O_3 changes little at 2–5 km above both sites on May 28–29 after switching off NA anthropogenic emissions (green lines in Figure 5), supporting a dominant source from the stratosphere as inferred from the O_3S tracer.

[33] We next examine transport of this enhanced O_3 aloft to the surface over the greater Los Angeles area and further

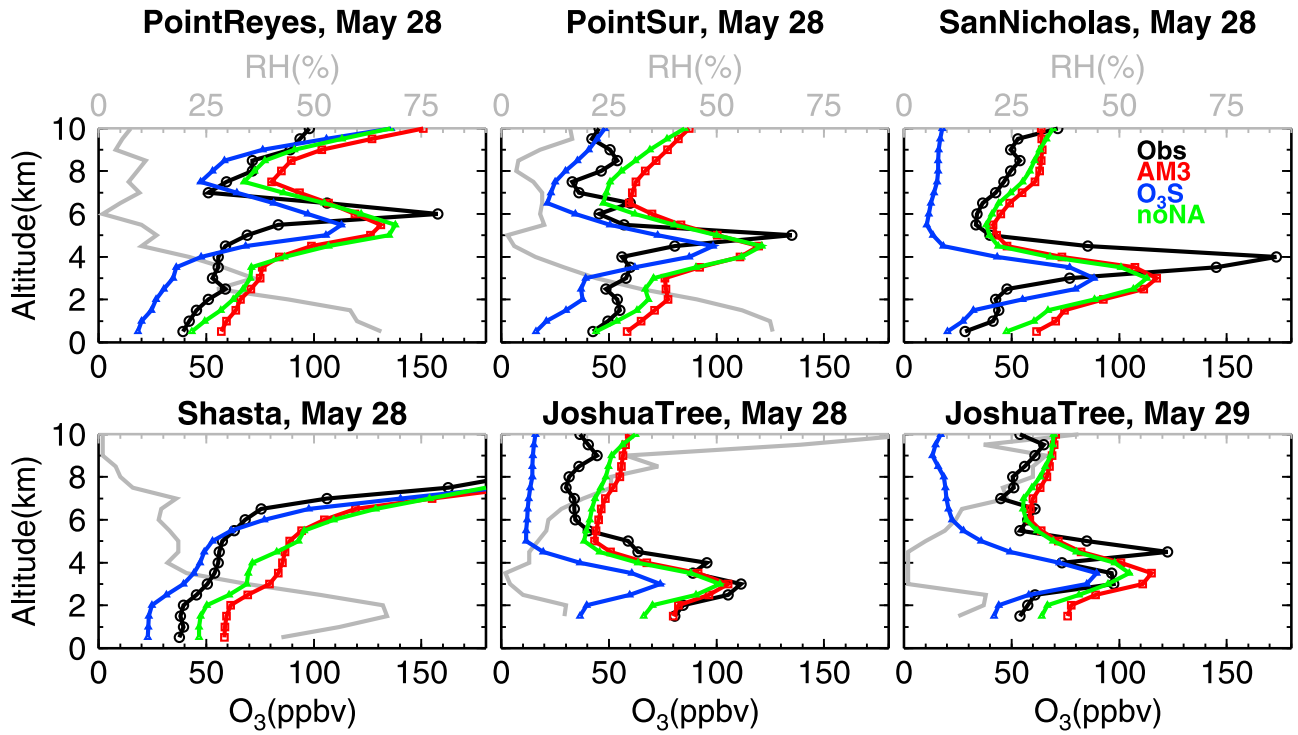

Figure 5. Same as Figure 3, but for the May 27–29 intrusion. Synoptic conditions for this intrusion are shown in Figure S4 in auxiliary material Text S1.

east across the Mountain West. Figure 6a shows that surface O_3 mixing ratios at Joshua Tree on May 28 and Mesa Verde on May 29 rapidly increase during the growth of daytime PBL coincident with a substantial decrease in specific humidity and colder afternoon temperature compared with other days. The timing of peak hourly O_3 gradually shifts from May 28 to May 29 at the surface sites from southern California to western Colorado, reflecting eastward transport of subsiding O_3 enriched, dry and cold air from the FT. These measured features support attribution to stratospheric origin based on AM3 O_3S for these observed surface O_3 enhancements (Figures 6b and 6c). At five sites where observed MDA8 O_3 reaches 77–82 ppbv (auxiliary material Table S1), exceeding the NAAQS threshold of 75 ppbv, the model estimates a stratospheric contribution of 35–55 ppbv, composing 50–60% of the total.

[34] Widespread entrainment of stratospheric O_3 into the boundary layer on May 29 led to ~10 ppbv increases in observed MDA8 O_3 over the entire Los Angeles area from the previous day (not shown). AM3 attributes a stratospheric contribution of 35–45 ppbv on May 29 (Figure 6c), representing the largest impacts over the Los Angeles area during CalNex, consistent with the PCA analysis by *Langford et al.* [2012]. The AM3 O_3S tracer over Southern California shows a deviation of up to 20–30 ppbv from monthly mean (Figure S5 in auxiliary material Text S1), similar to an O_3S tracer from the FLEXPART trajectory model that does not include stratospheric influence on the background [*Langford et al.*, 2012]. AM3 estimated a corresponding peak in O_3S mixing ratios on some days (e.g., May 20–22, May 28–29, June 10–11) when observed O_3 at Joshua Tree increases to 60–80 ppbv, implying that direct transport of stratospheric O_3 to the surface can occasionally enhance surface O_3 to levels near the NAAQS threshold over Southern California. We note that these stratospheric O_3 enhancements are smaller on highly polluted days, which are dominated by local influence from the Los Angeles area (e.g., June 4–5, when the stratospheric influence is weakest).

3.4. Stratospheric Influence Over the Four Corners Region: The May 22–24 and April 12–15 Intrusions

[35] We next present two cases of stratospheric intrusions primarily affecting surface O_3 over the Four Corners Region (Utah, Colorado, Arizona, and New Mexico). On the afternoon of May 23, the airborne lidar aboard the NOAA Twin Otter aircraft measured O_3 mixing ratios greater than 150 ppbv at ~4.5 km a.s.l. along a flight leg ~10 km south of Joshua Tree (Figure 7). AM3 reproduces this enhanced-O_3 layer and attributes a stratospheric contribution in excess of ~100 ppbv, indicating the penetration of an unusually large tropopause fold over Southern California. This tropopause fold was also measured by the ozonesondes on May 21–22 when it was located in the upper troposphere over Northern California (Figures S2 and S3 in auxiliary material Text S1).

[36] While ozonesonde or lidar measurements were not available to confirm the presence of the April 12–15 intrusion in the FT, the AIRS instrument onboard the NASA Aqua satellite captured a large-scale column enhancement of polar stratospheric O_3 extending to the U.S. West Coast on the afternoon of April 12 (Figure S1 in auxiliary material Text S1).

[37] Intrusions on both May 22–24 and April 12–15 contributed to elevated surface O_3 over the U.S. Mountain West and exceedances of the 75 ppbv NAAQS threshold at multiple sites (Figure 8). For both events, the GFDL AM3 model reproduces well the 60–85 ppbv range of observed surface

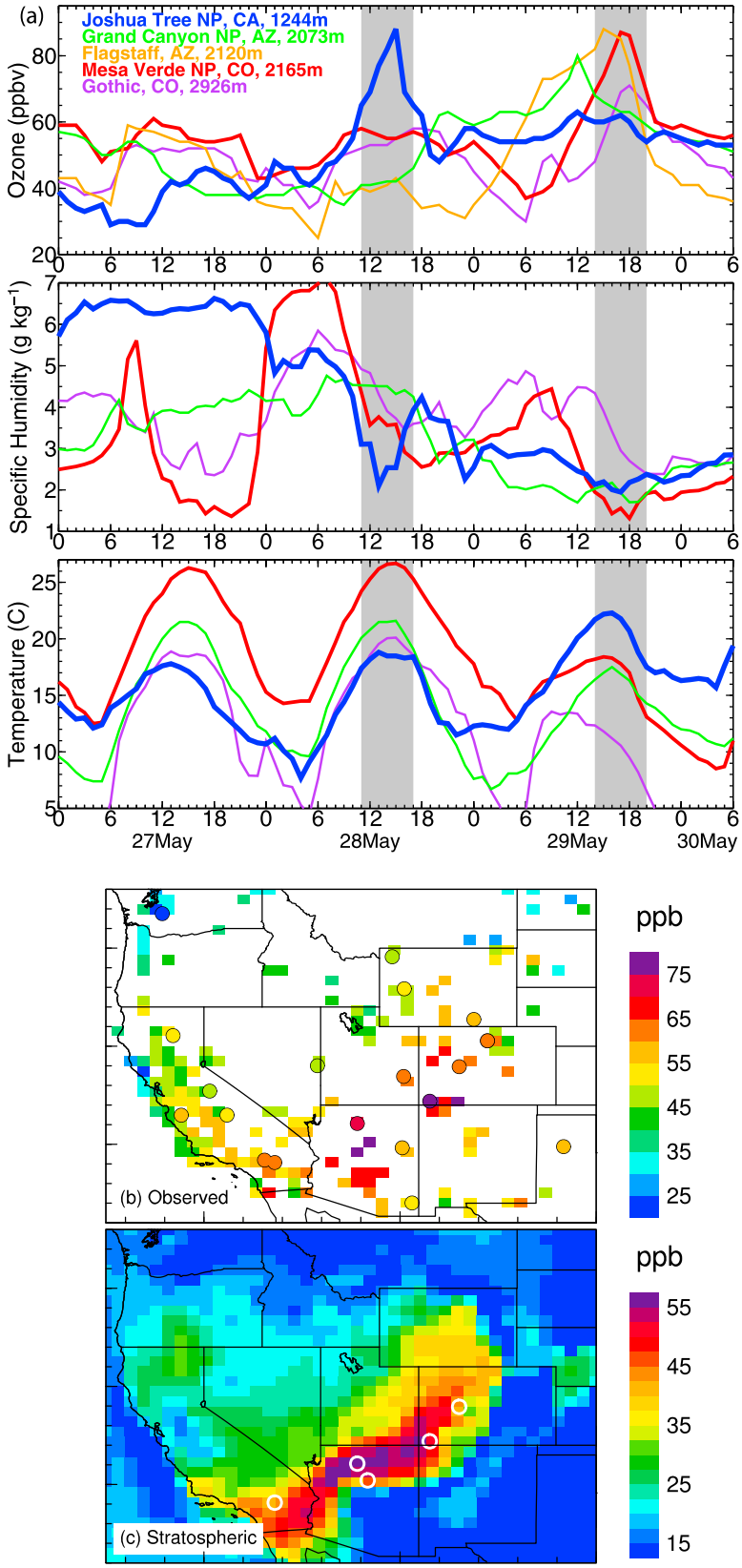

Figure 6. (a) Time series of observed hourly O_3 mixing ratios, specific humidity and temperature in surface air at the indicated stations from May 27–30, 2010. Note that humidity is not measured at Flagstaff. The gray shading masks the period at local time when the PBL is well mixed. (b) Total observed daily maximum 8-h average O_3 in surface air and (c) the AM3 simulated stratospheric O_3 tracer (in ppbv) on May 29, 2010. The white circles in Figure 6c denote the surface sites shown in Figure 6a.

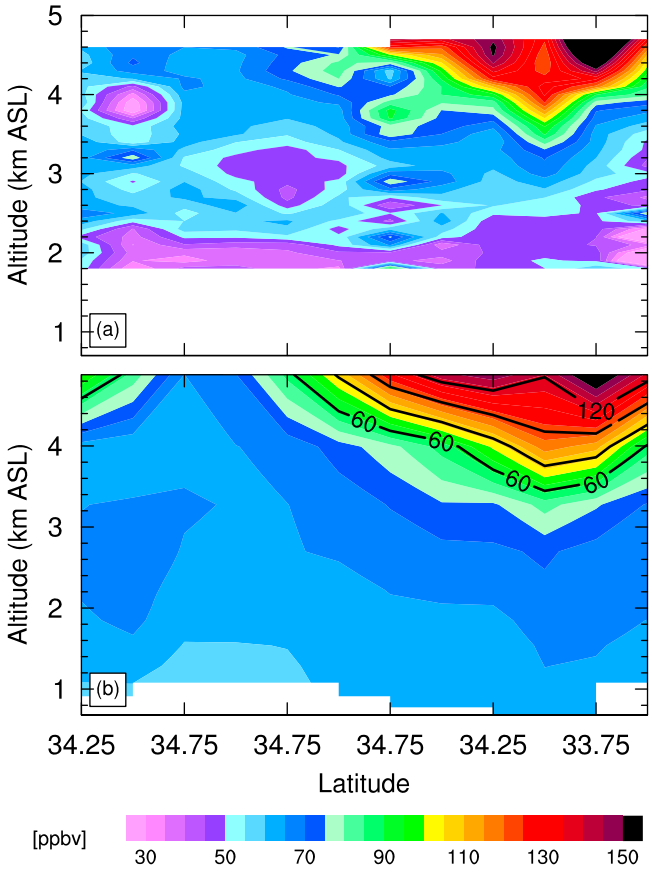

Figure 7. Latitude-height curtain plots of O_3 mixing ratios over Southern California for May 23 as (a) measured by an aircraft-based lidar (Figure 1) and (b) simulated by the GFDL AM3 model. Also shown is AM3 stratospheric O_3 tracer contoured every 20 ppbv starting at 60 ppbv. Synoptic conditions for this intrusion are shown in Figure S2 in auxiliary material Text S1.

O_3 at 25 urban and rural sites and estimates approximately 50–75 ppbv of O_3 in the absence of NA anthropogenic emissions (green points). The O_3S tracer (blue points) indicates that ~50% of the NA background is of stratospheric origin.

[38] The April 12–15 intrusion was the strongest intrusion during April–June 2010 affecting the surface areas over Colorado. Thirteen surface monitoring sites in Boulder, Denver and Colorado Springs, including six sites in metropolitan areas, experienced peak MDA8 O_3 concentrations greater than or equal to the 75 ppbv NAAQS threshold during April 13–15 on days when O_3S indicates a stratospheric contribution of 40–55 ppbv (Figure 8d). This intrusion pushed MDA8 O_3 concentrations to 79–86 ppbv at eight monitoring sites on 13–14 April 2010 (auxiliary material Table S1), comparable to the extreme case on 6 May 1999 described by *Langford et al.* [2009].

3.5. Overall Stratospheric Impacts on Surface Ozone Variability

[39] Time series of MDA8 O_3 from April–June 2010 at high-elevation western U.S. sites reveal thirteen observed episodes of 2–3 day duration where MDA8 O_3 > 70 ppbv are associated with increasing O_3S in the model surface layer (Figure 9 and Table 1). These high-O_3 events typically occurred in dry and cold conditions based on meteorological measurements at the CASTNet sites (e.g., Figure 6a), supporting attribution to stratospheric origin by the AM3 O_3S tracer. Despite variations in individual events, consistent synoptic patterns in the satellite images and reanalysis data confirm the occurrence of favorable meteorological conditions during all thirteen events for transporting stratospheric O_3 to the surface, either directly within a deep intrusion or indirectly from an intrusion that occurred in the mid- and upper troposphere with subsequent descent of O_3 enriched air to the surface. These intrusions, when combined with other sources of O_3, led to a total of 27 exceedances of the 75 ppbv NAAQS threshold for ground-level O_3.

[40] There is a marked case-to-case variability in the intensity and surface destination once stratospheric O_3 within an intrusion becomes irreversibly mixed into the troposphere. Only a very deep trough that traverses the California coast is likely to influence the southwestern U.S. surface, a phenomenon that was particularly active in the late spring and early summer of 2010 (Section 3.1). Our analysis indicates that surface O_3 enhancements from stratospheric intrusions are not restricted to the central western and northern U.S. as noted by several studies [e.g., *Langford et al.*, 2009; *Lefohn et al.*, 2011] but occasionally elevate surface O_3 as far south as the U.S. southwestern border. For example, the AQS site (~2 km a.s.l.) near Silver City in southern New Mexico recorded peak MDA8 O_3 of 70–80 ppbv 1–2 days after the passage of upper-level troughs, coincident with rising O_3S mixing ratios in the model (Figure 9, right). Two days after the May 11 intrusion measured in the free troposphere above California [*Langford et al.*, 2012; *Neuman et al.*, 2012], observed MDA8 O_3 exceeded 70 ppbv at Big Bend National Park in Southwestern Texas, representing the southernmost surface impacts from stratospheric intrusions during CalNex.

[41] Figure 9 shows that the GFDL AM3 model generally captures observed synoptic variability of MDA8 O_3 in surface air from April through June, which is dominated by background influence (primarily stratospheric O_3 intrusions) rather than by regional pollution. Correlation coefficients of simulated MDA8 O_3 with observations range from 0.42 to 0.74. Correlating the NA background directly with observations indicates that most of the variability is driven by fluctuations in the background (r = 0.32–0.62), and much of this background variability is due to variations in stratospheric influence (r = 0.19–0.66). At several sites (e.g., GRB, GRC, CAN), the higher correlation of NA background with observations as compared to O_3S reflects the influence of Asian pollution events (e.g., May 8–9 and June 20–22) [*Lin et al.*, 2012]. The role of STT variability on simulated surface O_3 over the Western U.S. in the model is even larger, with transport of stratospheric O_3 to the surface explaining ~40–80% of day-to-day variability of O_3 in the model.

4. Overall GFDL AM3 Evaluations

4.1. Stratospheric Intrusion Processes

[42] On the basis of the process-oriented evaluation in Section 3, we conclude that the GFDL AM3 model with

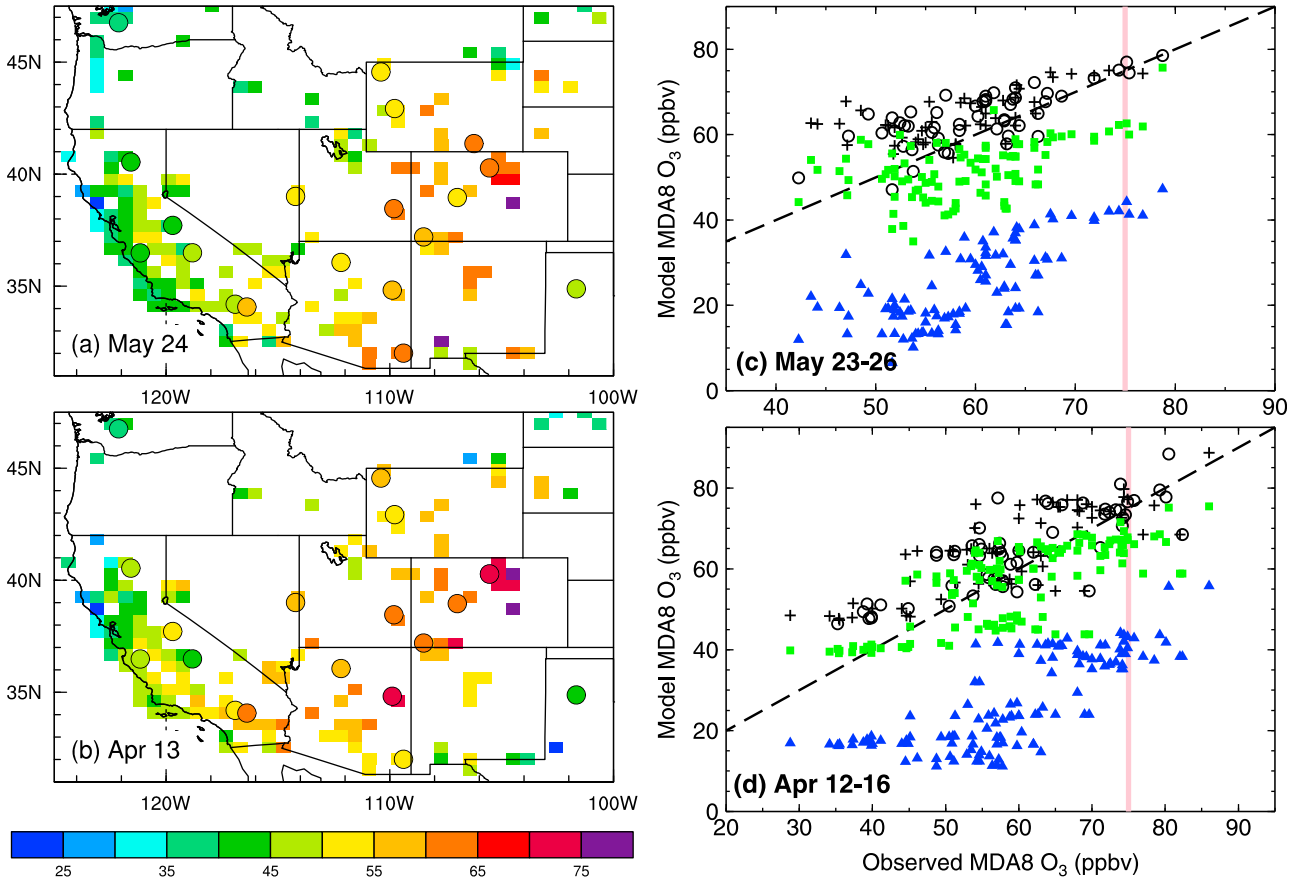

Figure 8. (a and b) Observed daily maximum 8-h average (MDA8) O_3 in surface air on May 24 and April 13. (c and d) Scatterplots of observed versus simulated MDA8 O_3 (black) as well as corresponding contributions from stratospheric intrusions (blue) and NA background (green, Section 2.2) at 25 sites where peak MDA8 values exceed 60 ppbv during May 23–26 and April 12–16. Black crosses indicate 9 urban/suburban sites located in Denver, Boulder, and Colorado Springs, with black circles indicating rural sites. Also shown is the 1:1 line (black dashes) and the NAAQS threshold (pink).

$\sim$50 $\times$ 50 km^2 horizontal resolution, nudged to GFS winds, reproduces the principal features of deep stratospheric intrusions, including the evolution of synoptic conditions, the descent of detached stratospheric O_3 to the lower troposphere, and its impacts on episodes of elevated O_3 in surface air. Specifically, AM3 resolves the filamentary features of stratospheric intrusions observed in the satellite imagery (Figure 2, Figures S1–S4 in auxiliary material Text S1, and *Lin et al.* [2012]), indicating the nudging technique succeeds in capturing the synoptic conditions controlling the observed distributions. Analysis of ozonesonde and lidar measurements (Figures 3, 5, and 7) demonstrates that AM3 reproduces the observed layered structure, sharp O_3 gradients of deep intrusions and associated day-to-day variability of O_3 over the western U.S. mid- and lower troposphere, a marked improvement upon previous models [e.g., *Roelofs et al.*, 2003; *Hudman et al.*, 2004; *Liang et al.*, 2007].

[43] The e90-based O_3S tracer tagging technique (Section 2.3) provides a robust method for estimating the contribution of STT to tropospheric O_3. For example, the greatest concentrations of O_3S tracer in the troposphere typically occur at the altitudes where observed RH suggests influence of dry air from the stratosphere. These intrusion layers also coincide with the enhanced background (green lines in Figures 3 and 5), which is dominated by the stratospheric contribution but estimated independent of the O_3S tagging technique.

[44] AM3 has a tendency to overestimate O_3 both in the upper troposphere (e.g., first row of Figures 3 and 5) and lower troposphere (e.g., fourth row of Figure 3). The layers with the peak O_3 enhancements in the model appear to be wider in thickness and lower in altitude than observed by the sondes. It is likely that the model is not adequately resolving the vertical structure of the intrusion layers, which could lead to excessive transport of stratospheric O_3 to the lower troposphere. We thus attempt to bias correct the AM3 estimates for surface O_3 (Section 5).

4.2. Surface Ozone

[45] The ability of AM3 to capture episodes of high-O_3 in excess of 70 ppbv at remote mountain sites in spring (Figure 12) is much improved than previous models [*Emery et al.*, 2012; *Zhang et al.*, 2011]. Mean surface O_3 in AM3 is biased high by $\sim$6 ppbv (Table 2). During observed high-O_3 episodes, there is no evidence for a systematic model bias in surface O_3 over the Rocky Mountains in Wyoming and Northern Colorado (Figure 9, left). In contrast, the model overestimates the observed MDA8 values by up to 10–20 ppbv in Arizona and New Mexico, which seems to reflect

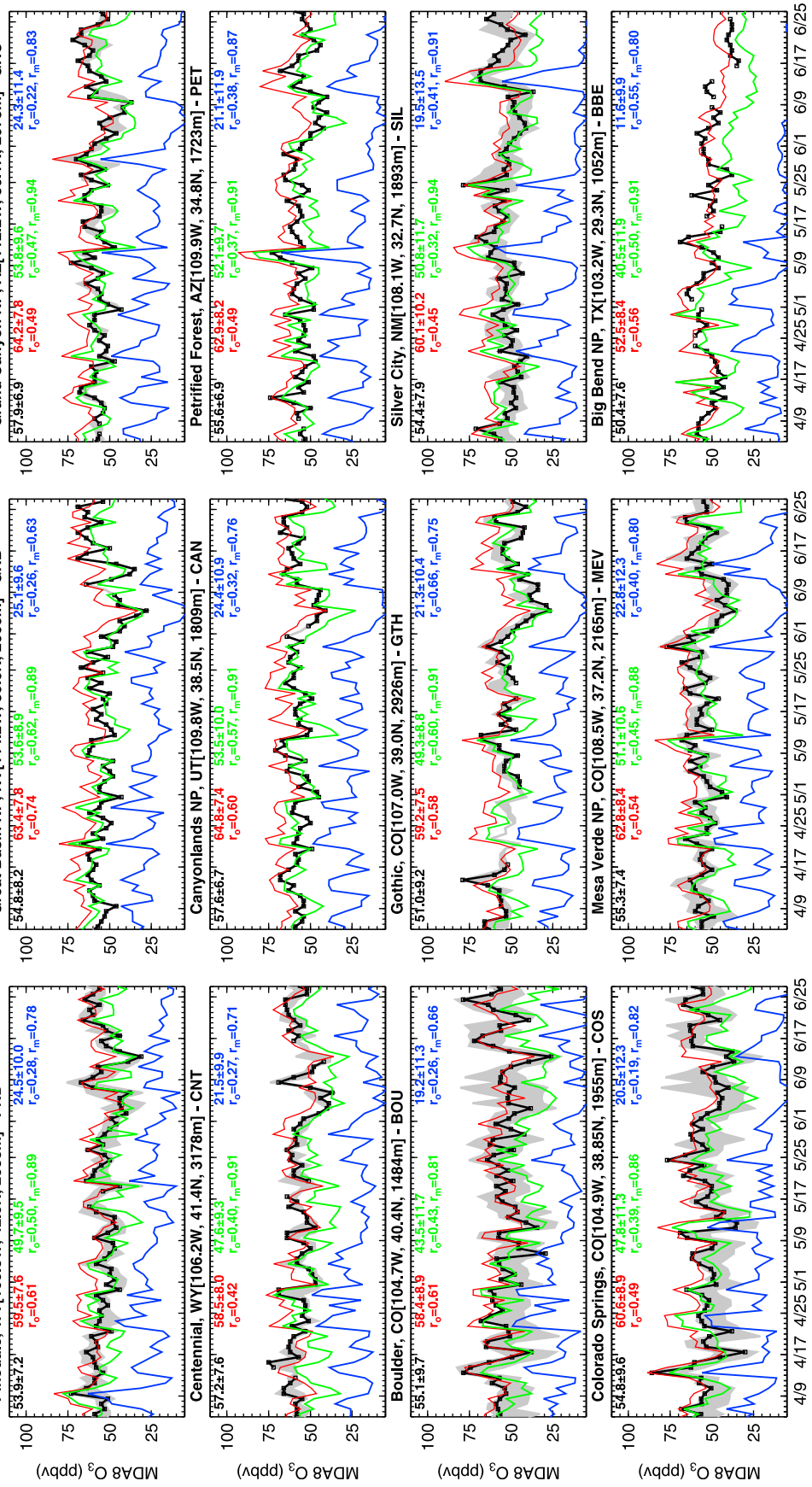

Figure 9. Time series of daily maximum 8-h average O_3 in surface air at western U.S. sites (Figure 1) for April through June 2010 as observed (black) and simulated (red) by the GFDL AM3 model. The gray shading represents range of any O_3 observations available within ~100 km from the selected site. Also shown are the model estimates for NA background (green) and the stratospheric contribution (blue), mean ± standard deviations, and their correlation coefficients with observed (r_o) and simulated (r_m) total O_3, respectively.

Table 2. Surface MDA8 Ozone Concentrations (in ppbv) Averaged Over 15 High-Elevation Western U.S. Sites for April–June 2010

Sources	Mean	Mean for Days > 60 ppbv
Total observed	55.3 ± 8.3	65.1 ± 4.4
Total modeled	61.0 ± 8.6	66.0 ± 8.3
NA anthropogenic	11.0 ± 5.0	11.6 ± 5.3
Total background[a]	50.0 ± 10.6	54.5 ± 10.6
Asian anthropogenic[b]	4.7 ± 2.4	5.3 ± 2.6
Stratospheric	22.3 ± 11.5	25.4 ± 12.3

[a]Includes the contribution from Asian pollution and stratospheric O_3.
[b]Based on AM3 simulations as described by *Lin et al.* [2012].

excessive stratospheric influence (Figure 9 (right) and Figure S7 in auxiliary material Text S1). The model typically spreads the O_3 enhancement across a wider range of sites over the Southwest rather than capturing the observed localized feature (e.g., April 6–7). The model has difficulty capturing the timing and placement of peak stratospheric impacts in surface air for some events (e.g., Figure 4). While the source of this problem is difficult to fully attribute, it may reflect some combined influences from limited resolution of sharp topography and meso-scale meteorology, inadequate representation of PBL dynamics, or missing O_3 sinks. For example, the current version of AM3 does not include the influence of halogens as a sink of surface O_3 [e.g., *Dickerson et al.*, 1999; *Keene et al.*, 2009; *Oltmans et al.*, 2012], which could decrease O_3 in northern midlatitude spring by ~4 ppb [*Parrella et al.*, 2012].

[46] We next evaluate the AM3 O_3 diurnal cycle (Figure 10). The model generally reproduces the diurnal variation of observed O_3, but tends to overestimate O_3 at 18:00–6:00 local time following an intrusion (e.g., at Mesa Verde and Silver City). This nighttime bias could reflect excessive entrainment of stratospheric O_3 given the model's difficulty representing shallow, stable nighttime boundary layer as noted in *Seidel et al.* [2012], or insufficient nighttime O_3 loss in the shallow boundary layer. Missing meso-scale features such as nocturnal low-level jets [e.g., *Whiteman et al.*, 1997] in the model may also contribute to the high nighttime O_3 bias.

[47] We expect that AM3 surface O_3 bias has greater influence on the uncertainty of our estimated stratospheric contribution to the baseline level than to the episodic enhancements in MDA8 O_3 for strong and deep intrusions. Figure S6 in auxiliary material Text S1 shows that our estimated stratospheric influence is moderately correlated (r^2 = 0.38–0.46) with model biases when observed MDA8 O_3 exceeds 60 ppbv. The correlation does not necessarily indicate a systematic model overestimate of stratospheric

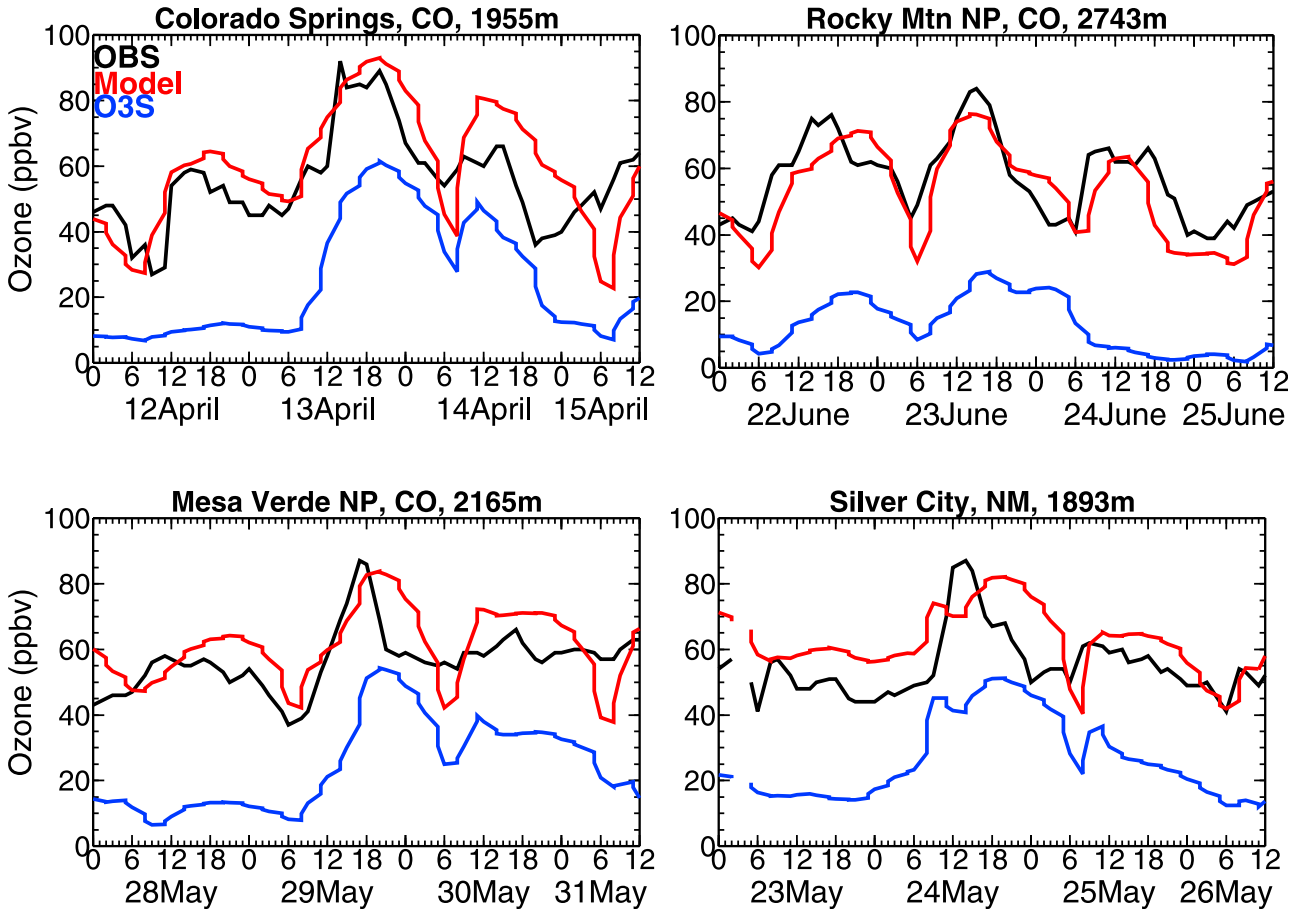

Figure 10. Hourly O_3 mixing ratios (in ppbv) at the indicated stations at local time during four intrusion events, showing total observed (black) and simulated (red) O_3 and the simulated stratospheric O_3 tracer (blue).

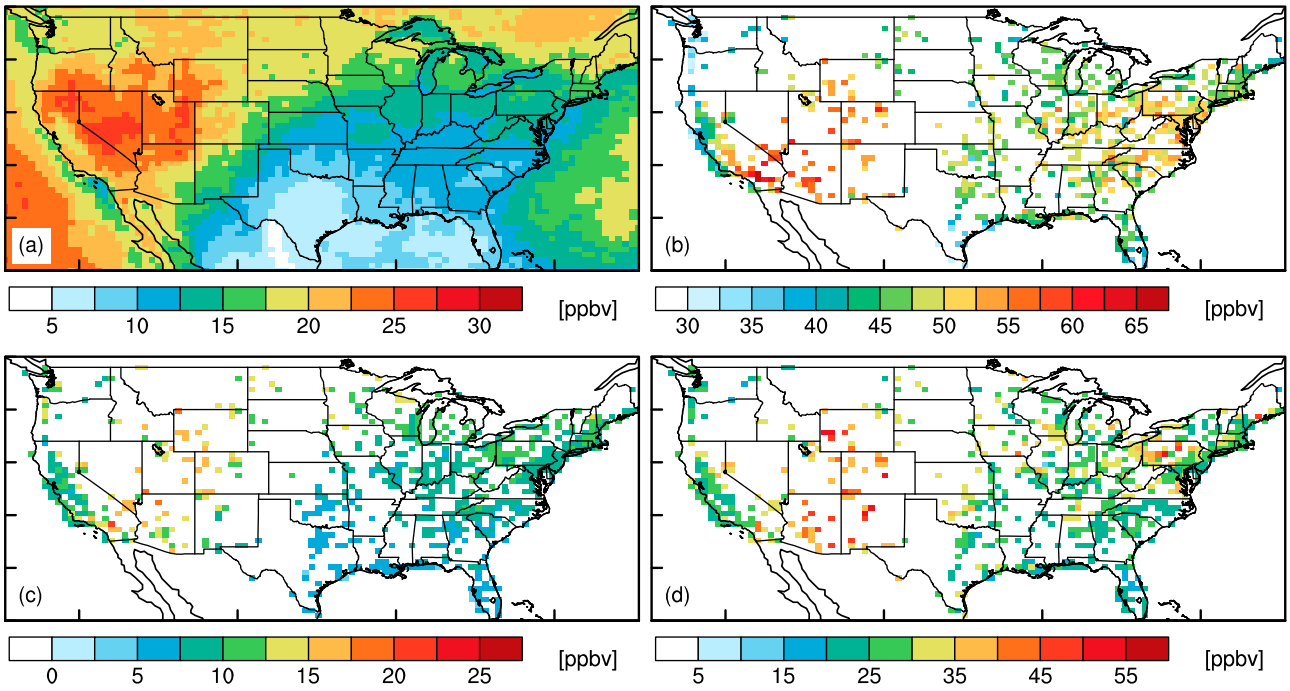

Figure 11. Continental U.S. distributions of (a) median stratospheric contribution to MDA8 surface O_3 from April–June 2010 as estimated by the GFDL AM3 model, (b) median MDA8 surface O_3 from AQS observations on the same 0.625° × 0.5° grid for AM3, and (c and d) bias-corrected estimates of the median and maximum stratospheric contribution (Section 4.2). Note the different color scale used to highlight regional variability.

contribution to high-O_3 events as both under- and overestimates occur. Indeed, the r^2 values decrease to 0.18–0.26 for all points with positive biases.

5. Statistics of Stratospheric Impacts on U.S. Surface Ozone in Spring

[48] We summarize in this section the overall statistics of stratospheric impacts on springtime ground-level O_3 drawing upon more than 10,000 samples of MDA8 O_3 measurements and model results from April–June 2010 (Figures 11 and 12). We attempt to remove the influence of excessive STT (such as may occur due to problems with resolving the timing and spatial location of deep intrusions, particularly in the SW region) in the lower troposphere and surface air. In places where we have observational constraints, we apply a bias correction to the simulated stratospheric and NA background contributions to surface O_3. For each day, at all sites where AM3 overestimates observed MDA8 O_3 and where the estimated stratospheric contribution exceeds the model bias, we assume that the bias is caused entirely by excessive stratospheric O_3. We thus subtract this bias from the AM3 estimate of stratospheric O_3 and NA background. The results thus represent a conservative estimate for stratospheric influence on surface O_3 since we do not correct for underestimates, and other processes, including regionally produced O_3, may contribute to the bias.

5.1. Regional Variability Across the Continental United States

[49] Figure 11a shows that the western U.S. is the region where STT contributes most to surface O_3 concentrations in spring, reflecting a combination of the higher frequency of deep intrusions off the west coast [*Sprenger and Wernli*, 2003] and the higher western topography that can intersect stratospheric O_3 subsiding behind cold fronts more readily than over the lower elevation eastern U.S. The minimum stratospheric influence in surface air occurs in the Southeast, where air masses advected from the Gulf of Mexico limit influence from westerly transport in the lower troposphere [*Fiore et al.*, 2002; *Cooper et al.*, 2011]. Within the western U.S., the model suggests strong stratospheric impacts on the Sierra Nevada mountain range and Nevada Air Basins, where monitoring sites are fairly sparse (Figure 11b). Measurements in these rural areas would help improve our understanding of stratospheric influence on O_3 air quality in nearby urban areas.

[50] The bias-corrected estimates of median stratospheric impacts in surface air range from 10 to 22, 8–13, and 3–8 ppbv in the West, Northeast, and Southeast, respectively (Figure 11c). The western states, including Wyoming, Utah, Colorado, Southern California, Arizona, and New Mexico, are subject to a maximum stratospheric impact of 35–55 ppbv (50–60% of the total) on MDA8 O_3 during the intrusions as discussed in Section 3 (Figure 11d). The average stratospheric contribution to western U.S. surface O_3 from April through June in AM3 is 20–30%. These AM3 estimates are a factor of 2–3 greater than the estimate of *Fiore et al.* [2003] (both average and episodically), and approximately 30–50% higher than the estimates of mean stratospheric influence by *Lelieveld and Dentener* [2000] and *Collins et al.* [2003] for the western U.S. in spring.

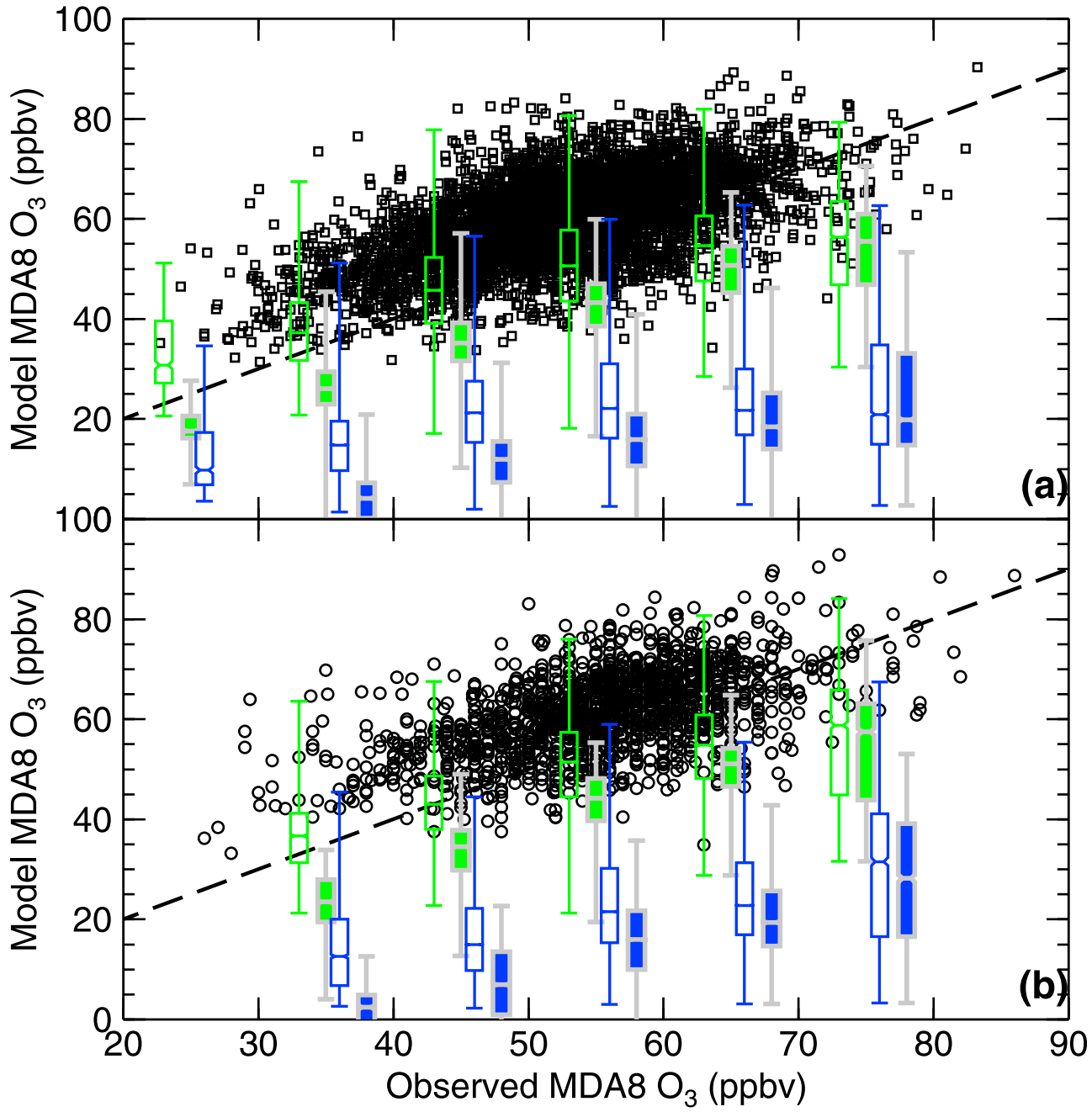

Figure 12. Model versus observed MDA8 surface O_3 for April–June 2010 at (a) AQS sites in EPA Region 8 and (b) 15 high-elevation sites (Figure 1). Also shown is the 1:1 line. The box-and-whisker plots (minimum, 25th, 50th, 75th percentiles, and maximum) give statistics of the NA background (green) and the stratospheric contribution (blue) for every 10-ppb bin of observed values. Points greater than 80 ppbv are merged to the 70–80 ppbv range. The filled boxes represent the bias-corrected estimates by assuming that model overestimates of total O_3 are entirely driven by excessive stratospheric influence (Section 5).

[51] The mean stratospheric contribution to surface O_3 over the eastern U.S. is lower than 15%. AM3 estimates a maximum stratospheric contribution of 30–45 ppbv at several scattered sites, supporting prior publications that deep STT can occasionally occur over this region [*Moody et al.*, 1998; *Sprenger and Wernli*, 2003; *Hocking et al.*, 2007; *Bourqui and Trepanier*, 2010; *Lefohn et al.*, 2011]. AM3 also suggests a significant surface contribution from STT (15–20 ppb in median) over the Western North Atlantic Ocean from April–June where the significance of stratospheric influence on surface O_3 at Bermuda has been debated [*Oltmans and Levy*, 1992; *Oltmans et al.*, 1996; *Moody et al.*, 1995; *Li et al.*, 2002]. Further process-oriented analysis as demonstrated in the present paper for the Western U.S. is needed to confidently assess the influence of deep STT on surface O_3 over these regions.

5.2. Contribution to Surface Ozone Distributions

[52] Next we assess the O_3 enhancements from stratospheric intrusions for the entire distribution of observed MDA8 O_3 over the intermountain west (Figure 12). Statistics of both original and bias-corrected AM3 estimates of the NA Background and the stratospheric contribution for each 10 ppbv bin of observed O_3 are shown. We focus on the bias-corrected estimates at the high end of the observed O_3 distribution, which has implications for the NAAQS-setting process.

[53] Both NA background O_3 and its stratospheric component peak at the high-end of the observed O_3 distribution for the high-elevation sites across the intermountain west (Figure 12b) as well as for the AQS sites in the central western U.S. (Figure 12a). At high-elevation sites, 25th–75th percentiles of stratospheric contribution range from 14 to 25 ppbv when observed MDA8 O_3 is 60–70 ppbv and increase to 17–40 ppbv in the 70–85 ppbv range. The median value of the stratospheric contribution at the AQS sites primarily within EPA Region 8 (Figure 1) is approximately 10 ppbv lower as compared to the high-elevation sites when observed O_3 is above 70 ppbv.

[54] For relatively polluted areas, such as the Central Valley, Southern California and Las Vegas, transport of stratospheric O_3 to the surface can mix with high levels of locally produced O_3 pollution. In these areas (Figure S8 in auxiliary material Text S1), NA background and its stratospheric component peak in the 60–80 ppbv range of observed O_3 and both tend to decline by 2–5 ppbv when observed O_3 is in the 80–100 ppbv range. This variability is qualitatively consistent with earlier work for the eastern U.S. [*e.g. Fiore et al.*, 2002, 2003].

[55] AM3 captures episodes of high-O_3 in excess of 70 ppbv at high-elevation western U.S. sites (Figure 12b). The background MDA8 O_3 concentration can reach 60–75 ppbv (bias-corrected; above the 75th percentile) and in these cases is primarily driven by stratospheric O_3. In contrast, two recent model estimates by *Zhang et al.* [2011] and *Emery et al.* [2012], show that the NA background is always below 60–65 ppbv. The median value of NA background when observed O_3 exceeds 70 ppbv is also ~10 ppbv greater in AM3 estimates than their model estimates.

[56] Table 2 shows that AM3 captures the observed O_3 values in excess of 60 ppbv at high-elevation sites, and estimates a total background contribution of 83% and a North American anthropogenic contribution of 17%. The stratospheric contribution and Asian pollution comprise 39% and 8% of the total, respectively. The dominant contribution from stratospheric O_3, and larger impacts with increasing O_3, indicates an important role for stratospheric intrusions in driving springtime surface high-O_3 events at western U.S. high-elevation sites.

6. Discussion and Conclusions

[57] To determine the extent to which naturally occurring stratospheric O_3 intrusions contribute to O_3 levels above the 75 ppb threshold for the U.S. National Ambient Air Quality Standard (NAAQS), we analyzed a wide range of satellite and in situ observations over the western U.S. from April–June 2010 utilizing a global chemistry-climate model at ~50 × 50 km^2 (GFDL AM3) [*Lin et al.*, 2012]. While *Lefohn et al.* [2001, 2011] and *Langford et al.* [2009, 2012] have used observations and trajectory models to infer a stratospheric influence on surface O_3 events, here we quantify that influence with a new stratospheric O_3 tracer (O_3S, Section 2.3) implemented in GFDL AM3 with fully coupled stratosphere-troposphere chemistry [*Donner et al.*, 2011; Naik et al., submitted manuscript, 2012].

[58] Our process-oriented analysis shows that AM3 reproduces the principal features of deep stratospheric intrusions. Specifically, it captures the evolution of synoptic conditions, the descent of stratospheric O_3 to the lower troposphere as evidenced by its replication of the layered structures and sharp gradients observed in O_3 profiles (Figures 3–7), and the development of high-O_3 events observed in surface air (Figure 8). The good agreement builds confidence in the utility of AM3 for identifying "exceptional stratospheric intrusion events" that elevate surface O_3 to values above the NAAQS threshold [*U.S. EPA*, 2007; *Langford et al.*, 2009]. The most significant weakness of the model is a high surface O_3 bias of ~6 ppbv on average, which may reflect some combined influence from missing O_3 sinks and model limitations in resolving meso-scale meteorology and nighttime PBL. We correct the AM3 estimate of stratospheric O_3 contribution to account for this model bias by conservatively assuming that the model overestimates at ground-based measurement sites are entirely driven by excessive stratospheric O_3 influence (Section 5).

[59] We show that transport of stratospheric O_3 to the surface can drive a substantial portion of the observed synoptic variability in western U.S. surface O_3 (Figures 4 and 9). Thirteen stratospheric intrusion events, occurring approximately weekly from April–June 2010 (Table 1), enhanced total observed MDA8 O_3 to ~70–86 ppbv at surface sites. A total of 27 exceedances of the 75-ppbv NAAQS threshold occurred during six of these events, including several incidences in suburban areas of Arizona, Colorado and New Mexico. During four deep intrusion events (April 12–15, May 22–24, May 27–29, and June 7–8), transport of stratospheric O_3 to the surface can elevate MDA8 O_3 by 20–40 ppbv above the baseline level (Figure 9). Stratospheric influence accounts for 50–60% of the total O_3 in the model surface layer on days when observed O_3 exceeds the NAAQS O_3 threshold (e.g., Figures 4–8). A sensitivity simulation with NA anthropogenic emissions shut off in the model supports attribution to background. Both the background O_3 concentration and its stratospheric component peak at the high-end of the observed O_3 distribution over the U.S. Mountain West (Figure 12). At these high-elevation sites in springtime, stratospheric O_3 contributes more than O_3 produced from North American and Asian anthropogenic emissions (Table 2).

[60] AM3 estimates of stratospheric impacts on springtime surface O_3 over the western U.S. is generally higher on average, and up to 2–3 times greater during the intrusions, than previous model estimates [e.g., *Lelieveld and Dentener*, 2000; *Collins et al.*, 2003; *Fiore et al.*, 2003; *Langford et al.*, 2012]. Our finding is in notable contrast to prior work concluding that stratospheric influence on high surface O_3 events is rare [e.g., *Fiore et al.*, 2003; *U.S. EPA*, 2007]. While some of the discrepancies may reflect the higher resolution of AM3 and interannual variability associated with ENSO and other factors (Section 3.1), the AM3 explicit

simulation of O_3 variability in the lower stratosphere and its dynamic coupling with the troposphere (Section 2.2), as opposed to using SYNOZ (e.g., as in *Fiore et al.* [2003]) or a climatological stratosphere [e.g., *Hess and Lamarque*, 2007; *Pfister et al.*, 2008], is likely the major reason for the improved simulation of episodic STT impacts upon previous models.

[61] Prior work has shown a dependence on the attribution of mean stratospheric impacts to the different O_3S tagging methods used [e.g., *Hess and Lamarque*, 2007]. We expect less sensitivity for deep intrusion events such as those focused on here (Section 2.3) and the use of the dynamic e90 tracer in AM3 represents a major improvement. It should be emphasized that AM3 simulations of total O_3 and background O_3 (eliminating NA anthropogenic influence), which reproduces observed O_3 enhancements both in surface air and aloft during the intrusions, are independent of the tagging method. Given the policy implications, it is important for future modeling work to reproduce our findings. We suggest an intercomparison of a wide range of models, including those with fully coupled stratosphere-troposphere chemistry and dynamics (as with AM3), that apply consistent O_3S tagging methods as a first step.

[62] Our analysis implies that episodic stratospheric intrusions may pose a challenge for springtime O_3 over the U.S. Mountain West to stay below the O_3 NAAQS with domestic emission controls, particularly if a threshold value in the 60–70 ppbv range were to be adopted [*U.S. EPA*, 2010]. We underscore that O_3 produced from local emissions dominates O_3 pollution in urban areas, in lower elevation U.S. regions, and during summer. Nevertheless, STT may influence surface O_3 over other midlatitude regions prone to deep intrusions, such as the western North Atlantic Ocean region and western Europe where meteorological conditions similar to the western U.S. occur [e.g., *Moody et al.*, 1995; *Appenzeller et al.*, 1996; *Sprenger and Wernli*, 2003]. Further, some climate models project a higher contribution of stratospheric exchange to tropospheric O_3 under future climate scenarios, presumably due to stratospheric O_3 recovery and an accelerated Brewer-Dobson circulation in a warmer climate [e.g., *Collins et al.*, 2003; *Austin and Wilson*, 2006; *Stevenson et al.*, 2006; *Hegglin and Shepherd*, 2009; *Zeng et al.*, 2010].

[63] **Acknowledgments.** This work is supported by the Cooperative Institute for Climate Science (CICS)–a collaboration between Princeton University and NOAA Geophysical Fluid Dynamics Laboratory (GFDL), and by the NASA Air Quality Applied Science Team (AQAST) (NNX12AF15G). Funding for the IONS-2010 field campaign was provided by NOAA ESRL Health of the Atmosphere Program, NASA Tropospheric Chemistry Program, U. S. Navy, Environment Canada and NOAA's National Air Quality Forecast Capability. Operations were facilitated by personnel from Joshua Tree National Park, Point Reyes National Seashore, Shasta State Historic Park, Point Sur State Historic Park, and the Naval Postgraduate School (NPS), Monterey. We are grateful to Zhiguo Zhang for help processing AQS data and to Paul Ginoux, Allen Lefohn, Bud Moxim, and Joe Pinto for discussions and comments on the manuscript. We thank three anonymous reviewers for constructive comments which we believe have helped to strengthen this paper.

References

Alvarez, R. J., II, et al. (2011), Development and application of a compact, tunable, solid-state airborne ozone lidar system for boundary layer profiling, *J. Atmos. Oceanic Technol.*, *28*, 1258–1272, doi:10.1175/JTECH-D-10-05044.1.

Appenzeller, C., and H. C. Davies (1992), Structure of stratospheric intrusions into the troposphere, *Nature*, *358*(6387), 570–572, doi:10.1038/358570a0.

Appenzeller, C., H. C. Davies, and W. A. Norton (1996), Fragmentation of stratospheric intrusions, *J. Geophys. Res.*, *101*(D1), 1435–1456, doi:10.1029/95JD02674.

Austin, J., and R. J. Wilson (2006), Ensemble simulations of the decline and recovery of stratospheric ozone, *J. Geophys. Res.*, *111*, D16314, doi:10.1029/2005JD006907.

Austin, J., and R. J. Wilson (2010), Sensitivity of polar ozone to sea surface temperatures and halogen amounts, *J. Geophys. Res.*, *115*, D18303, doi:10.1029/2009JD013292.

Bourqui, M. S., and P.-Y. Trepanier (2010), Descent of deep stratospheric intrusions during the IONS August 2006 campaign, *J. Geophys. Res.*, *115*, D18301, doi:10.1029/2009JD013183.

Bowman, K. P., L. L. Pan, T. Campos, and R.-S. Gao (2007), Observations of fine-scale transport structure in the upper troposphere from HIAPER, *J. Geophys. Res.*, *112*, D18111, doi:10.1029/2007JD008685.

Browell, E. V., E. F. Danielsen, S. Ismail, G. L. Gregory, and S. M. Beck (1987), Tropopause fold structure determined from airborne lidar and in situ measurements, *J. Geophys. Res.*, *92*, 2112–2120, doi:10.1029/JD092iD02p02112.

Collins, W. J., R. G. Derwent, B. Garnier, C. E. Johnson, M. G. Sanderson, and D. S. Stevenson (2003), Effect of stratosphere-troposphere exchange on the future tropospheric ozone trend, *J. Geophys. Res.*, *108*(D12), 8528, doi:10.1029/2002JD002617.

Cooper, O. R., J. L. Moody, J. C. Davenport, S. J. Oltmans, B. J. Johnson, X. Chen, P. B. Shepson, and J. T. Merrill (1998), Influence of springtime weather systems on vertical ozone distributions over three North American sites, *J. Geophys. Res.*, *103*, 22,001–22,013.

Cooper, O. R., J. L. Moody, D. D. Parrish, M. Trainer, T. B. Ryerson, J. S. Holloway, G. Hübler, F. C. Fehsenfeld, S. J. Oltmans, and M. J. Evans (2001), Trace gas signatures of the airstreams within North Atlantic cyclones: Case studies from the NARE'97 aircraft intensive, *J. Geophys. Res.*, *106*(D6), 5437–5456, doi:10.1029/2000JD900574.

Cooper, O. R., et al. (2004), On the life cycle of a stratospheric intrusion and its dispersion into polluted warm conveyor belts, *J. Geophys. Res.*, *109*, D23S09, doi:10.1029/2003JD004006.

Cooper, O. R., et al. (2005), Direct transport of mid-latitude stratospheric ozone into the lower troposphere and marine boundary layer of the tropical Pacific Ocean, *J. Geophys. Res.*, *110*, D23310, doi:10.1029/2005JD005783.

Cooper, O. R., et al. (2011), Measurement of western U.S. baseline ozone from the surface to the tropopause and assessment of downwind impact regions, *J. Geophys. Res.*, *116*, D00V03, doi:10.1029/2011JD016095.

Danielsen, E. F. (1968), Stratospheric-tropospheric exchange based on radioactivity, ozone and potential vorticity, *J. Atmos. Sci.*, *25*, 502–518, doi:10.1175/1520-0469(1968)025<0502:STEBOR>2.0.CO;2.

Danielsen, E. F., R. S. Hipskind, S. E. Gaines, G. W. Sachse, G. L. Gregory, and G. F. Hill (1987), Three-dimensional analysis of potential vorticity associated with tropopause folds and observed variations of ozone and carbon monoxide, *J. Geophys. Res.*, *92*(D2), 2103–2111, doi:10.1029/JD092iD02p02103.

Dickerson, R. R., K. P. Rhoads, T. C. Carsey, S. J. Oltmans, J. P. Burrows, and P. J. Crutzen (1999), Ozone in the remote marine boundary layer: A possible role for halogens, *J. Geophys. Res.*, *104*, 21,385–21,395, doi:10.1029/1999JD900023.

Ding, A., and T. Wang (2006), Influence of stratosphere-to-troposphere exchange on the seasonal cycle of surface ozone at Mount Waliguan in western China, *Geophys. Res. Lett.*, *33*, L03803, doi:10.1029/2005GL024760.

Donner, L. J., et al. (2011), The dynamical core, physical parameterizations, and basic simulation characteristics of the atmospheric component AM3 of the GFDL Global Coupled Model CM3, *J. Clim.*, *24*, 3484–3519, doi:10.1175/2011JCLI3955.1.

Emery, C., J. Jung, N. Downey, J. Johnson, M. Jimenez, G. Yarwood, and R. Morris (2012), Regional and global modeling estimates of policy relevant background ozone over the United States, *Atmos. Environ.*, *47*, 206–217, doi:10.1016/j.atmosenv.2011.11.012.

Emmons, L. K., et al. (2003), Budget of tropospheric ozone during TOPSE from two chemical transport models, *J. Geophys. Res.*, *108*(D8), 8372, doi:10.1029/2002JD002665.

Emmons, L. K., et al. (2010), Description and evaluation of the Model for Ozone and Related chemical Tracers, version 4 (MOZART-4), *Geosci. Model Dev.*, *3*, 43–67, doi:10.5194/gmd-3-43-2010.

Felker, S. R., J. L. Moody, A. J. Wimmers, G. Osterman, and K. Bowman (2011), A Multi-sensor Upper Tropospheric Ozone Product (MUTOP) based on TES ozone and GOES water vapor: Derivation, *Atmos. Chem. Phys.*, *11*, 6515–6527, doi:10.5194/acp-11-6515-2011.

Fiore, A. M., D. J. Jacob, I. Bey, R. M. Yantosca, B. D. Field, A. C. Fusco, and J. G. Wilkinson (2002), Background ozone over the United States in summer: Origin, trend, and contribution to pollution episodes, *J. Geophys. Res.*, *107*(D15), 4275, doi:10.1029/2001JD000982.

Fiore, A., D. J. Jacob, H. Liu, R. M. Yantosca, T. D. Fairlie, and Q. Li (2003), Variability in surface ozone background over the United States: Implications for air quality policy, *J. Geophys. Res.*, *108*(D24), 4787, doi:10.1029/2003JD003855.

Hegglin, M. I., and T. G. Shepherd (2009), Large climate-induced changes in ultraviolet index and stratosphere-to-troposphere ozone flux, *Nat. Geosci.*, *2*, 687–691, doi:10.1038/ngeo604.

Hess, P. G., and J.-F. Lamarque (2007), Ozone source attribution and its modulation by the Arctic oscillation during the spring months, *J. Geophys. Res.*, *112*, D11303, doi:10.1029/2006JD007557.

Hocking, W. K., et al. (2007), Detection of stratospheric ozone intrusions by windprofiler radars, *Nature*, *450*, 281–284, doi:10.1038/nature06312.

Holton, J. R., P. H. Haynes, E. M. McIntyre, A. R. Douglass, R. B. Rood, and L. Pfister (1995), Stratosphere-troposphere exchange, *Rev. Geophys.*, *33*, 403–439, doi:10.1029/95RG02097.

Horowitz, L. W., et al. (2003), A global simulation of tropospheric ozone and related tracers: Description and evaluation of MOZART, version 2, *J. Geophys. Res.*, *108*(D24), 4784, doi:10.1029/2002JD002853.

Hsu, J., and M. J. Prather (2009), Stratospheric variability and tropospheric ozone, *J. Geophys. Res.*, *114*, D06102, doi:10.1029/2008JD010942.

Hsu, J., M. J. Prather, and O. Wild (2005), Diagnosing the stratosphere-to-troposphere flux of ozone in a chemistry transport model, *J. Geophys. Res.*, *110*, D19305, doi:10.1029/2005JD006045.

Hudman, R. C., et al. (2004), Ozone production in transpacific Asian pollution plumes and implications for ozone air quality in California, *J. Geophys. Res.*, *109*, D23S10, doi:10.1029/2004JD004974.

James, P., A. Stohl, C. Forster, S. Eckhardt, P. Seibert, and A. Frank (2003), A 15-year climatology of stratosphere-troposphere exchange with a Lagrangian particle dispersion model: 2. Mean climate and seasonal variability, *J. Geophys. Res.*, *108*(D12), 8522, doi:10.1029/2002JD002639.

Johnson, W. B., and W. Viezee (1981), Stratospheric ozone in the lower troposphere: I. presentation and interpretation of aircraft measurement, *Atmos. Environ.*, *15*, 1309–1323, doi:10.1016/0004-6981(81)90325-5.

Keene, W. C., et al. (2009), Latitudinal variation in the multiphase chemical processing of inorganic halogens and related species over the eastern North and South Atlantic Oceans, *Atmos. Chem. Phys.*, *9*, 7361–7385, doi:10.5194/acp-9-7361-2009.

Koumoutsaris, S., I. Bey, S. Generoso, and V. Thouret (2008), Influence of El Niño–Southern Oscillation on the interannual variability of tropospheric ozone in the northern mid-latitudes, *J. Geophys. Res.*, *113*, D19301, doi:10.1029/2007JD009753.

Lamarque, J.-F., and P. G. Hess (2004), Arctic Oscillation modulation of the Northern Hemisphere spring tropospheric ozone, *Geophys. Res. Lett.*, *31*, L06127, doi:10.1029/2003GL019116.

Langford, A. O., C. D. Masters, M. H. Proffitt, E. Y. Hsie, and A. F. Tuck (1996), Ozone measurements in a tropopause fold associated with a cut-off low system, *Geophys. Res. Lett.*, *23*(18), 2501–2504, doi:10.1029/96GL02227.

Langford, A. O., T. J. O'Leary, C. D. Masters, K. C. Aikin, and M. H. Proffitt (1998), Modulation of middle and upper tropospheric ozone at northern midlatitudes by the El Niño/Southern Oscillation, *Geophys. Res. Lett.*, *25*, 2667–2670, doi:10.1029/98GL01909.

Langford, A. O., K. C. Aikin, C. S. Eubank, and E. J. Williams (2009), Stratospheric contribution to high surface ozone in Colorado during springtime, *Geophys. Res. Lett.*, *36*, L12801, doi:10.1029/2009GL038367.

Langford, A. O., J. Brioude, O. R. Cooper, C. J. Senff, R. J. Alvarez II, R. M. Hardesty, B. J. Johnson, and S. J. Oltmans (2012), Stratospheric influence on surface ozone in the Los Angeles area during late spring and early summer of 2010, *J. Geophys. Res.*, *117*, D00V06, doi:10.1029/2011JD016766.

Lefohn, A. S., S. J. Oltmans, T. Dann, and H. B. Singh (2001), Present-day variability of background ozone in the lower troposphere, *J. Geophys. Res.*, *106*(D9), 9945–9958, doi:10.1029/2000JD900793.

Lefohn, A. S., et al. (2011), The importance of stratospheric-tropospheric transport in affecting surface ozone concentrations in the western and northern tier of the United States, *Atmos. Environ.*, *45*(28), 4845–4857, doi:10.1016/j.atmosenv.2011.06.014.

Lelieveld, J., and F. J. Dentener (2000), What controls tropospheric ozone?, *J. Geophys. Res.*, *105*(D3), 3531–3551, doi:10.1029/1999JD901011.

Levy, H., J. D. Mahlmann, W. J. Moxim, and S. C. Liu (1985), Tropospheric ozone: The role of transport, *J. Geophys. Res.*, *90*(D2), 3753–3772, doi:10.1029/JD090iD02p03753.

Li, Q., D. J. Jacob, T. D. Fairlie, H. Liu, R. V. Martin, and R. M. Yantosca (2002), Stratospheric versus pollution influences on ozone at Bermuda: Reconciling past analyses, *J. Geophys. Res.*, *107*(D22), 4611, doi:10.1029/2002JD002138.

Liang, Q., et al. (2007), Summertime influence of Asian pollution in the free troposphere over North America, *J. Geophys. Res.*, *112*, D12S11, doi:10.1029/2006JD007919.

Lin, M., et al. (2012), Transport of Asian ozone pollution into surface air over the western United States in spring, *J. Geophys. Res.*, *117*, D00V07, doi:10.1029/2011JD016961.

Lock, A. P., A. R. Brown, M. R. Bush, G. M. Martin, and R. N. B. Smith (2000), A new boundary layer mixing scheme. Part I: Scheme description and single column model tests, *Mon. Weather Rev.*, *128*, 3187–3199, doi:10.1175/1520-0493(2000)128<3187:ANBLMS>2.0.CO;2.

McDonald-Buller, E. C., et al. (2011), Establishing policy relevant background (PRB) ozone concentrations in the United States, *Environ. Sci. Technol.*, *45*(22), 9484–9497, doi:10.1021/es2022818.

McLinden, C. A., S. C. Olsen, B. Hannegan, O. Wild, M. J. Prather, and J. Sundet (2000), Stratospheric ozone in 3-D models: A simple chemistry and the cross-tropopause flux, *J. Geophys. Res.*, *105*(D11), 14,653–14,665, doi:10.1029/2000JD900124.

Monks, P. S. (2000), A review of the observations and origins of the spring ozone maximum, *Atmos. Environ.*, *34*, 3545–3561, doi:10.1016/S1352-2310(00)00129-1.

Moody, J. L., S. J. Oltmans, H. Levy II, and J. T. Merrill (1995), Transport climatology of tropospheric ozone: Bermuda, 1988–1991, *J. Geophys. Res.*, *100*(D4), 7179–7194, doi:10.1029/94JD02830.

Moody, J. L., J. W. Munger, A. H. Goldstein, D. J. Jacob, and S. C. Wofsy (1998), Harvard Forest regional-scale air mass composition by Patterns in Atmospheric Transport History (PATH), *J. Geophys. Res.*, *103*(D11), 13,181–13,194, doi:10.1029/98JD00526.

Moss, R. H., et al. (2010), The next generation of scenarios for climate change research and assessment, *Nature*, *463*, 747–756, doi:10.1038/nature08823.

National Research Council (NRC) (2009), *Global Sources of Local Pollution: An Assessment of Long-Range Transport of Key Air Pollutants to and From the United States*, 248 pp., Natl. Acad., Washington, D. C.

Neuman, J. A., et al. (2012), Observation of ozone transport from the free troposphere to the Los Angeles basin, *J. Geophys. Res.*, *117*, D00V09, doi:10.1029/2011JD016919.

Oltmans, S. J., and H. Levy II (1992), Seasonal cycle of surface ozone over the western North Atlantic, *Nature*, *358*, 392–394, doi:10.1038/358392a0.

Oltmans, S. J., et al. (1996), Summer and spring ozone profiles over the North Atlantic from ozonesonde measurements, *J. Geophys. Res.*, *101*(D22), 29,179–29,200, doi:10.1029/96JD01713.

Oltmans, S. J., B. J. Johnson, and J. M. Harris (2012), Springtime boundary layer ozone depletion at Barrow, Alaska: Meteorological influence, year-to-year variation, and long-term change, *J. Geophys. Res.*, *117*, D00R18, doi:10.1029/2011JD016889.

Parrella, J. P., et al. (2012), Tropospheric bromine chemistry: Implications for present and pre-industrial ozone and mercury, *Atmos. Chem. Phys.*, *12*, 6723–6740, doi:10.5194/acp-12-6723-2012.

Pfister, G., A. M. Thompson, L. K. Emmons, P. G. Hess, J.-F. Lamarque, and Y. E. Yorks (2008), Analysis of the Summer 2004 ozone budget over the United States using Intercontinental Transport Experiment Ozonesonde Network Study (IONS) observations and Model of Ozone and Related Tracers (MOZART-4) simulations, *J. Geophys. Res.*, *113*, D23306, doi:10.1029/2008JD010190.

Prather, M. et al. (2001), Atmospheric chemistry and greenhouse gases, in *Climate Change 2001: The Scientific Basis. Third Assessment Report of the Intergovernmental Panel on Climate Change*, edited by J. T. Houghton et al., pp. 239–287, Cambridge Univ. Press, Cambridge, U. K.

Prather, M. J., X. Zhu, Q. Tang, J. Hsu, and J. L. Neu (2011), An atmospheric chemist in search of the tropopause, *J. Geophys. Res.*, *116*, D04306, doi:10.1029/2010JD014939.

Price, J. D., and G. Vaughan (1993), The potential for stratosphere-troposphere exchange in cutoff-low systems, *Q. J. R. Meteorol. Soc.*, *119*, 343–365, doi:10.1002/qj.49711951007.

Roelofs, G.-J., and J. Lelieveld (1997), Model study of the influence of cross-tropopause O_3 transports on tropospheric O_3 levels, *Tellus, Ser. B*, *49*, 38–55, doi:10.1034/j.1600-0889.49.issue1.3.x.

Roelofs, G. J., et al. (2003), Intercomparison of tropospheric ozone models: Ozone transport in a complex tropopause folding event, *J. Geophys. Res.*, *108*(D12), 8529, doi:10.1029/2003JD003462.

Seidel, D. J., Y. Zhang, A. C. M. Beljaars, J.-C. Golaz, A. R. Jacobson, and B. Medeiros (2012), Climatology of the planetary boundary layer over the continental United States and Europe, *J. Geophys. Res.*, *117*, D17106, doi:10.1029/2012JD018143.

Shapiro, M. A. (1980), Turbulent mixing within tropopause folds as a mechanism for the exchange of chemical constituents between the stratosphere and troposphere, *J. Atmos. Sci.*, *37*, 994–1004, doi:10.1175/1520-0469(1980)037<0994:TMWTFA>2.0.CO;2.

Sprenger, M., and H. Wernli (2003), A northern hemispheric climatology of cross-tropopause exchange for the ERA15 time period (1979–1993), *J. Geophys. Res.*, *108*(D12), 8521, doi:10.1029/2002JD002636.

State of Colorado (2011), Technical support document for the May 24, 2010, stratospheric ozone intrusion exceptional event, report, Air Pollut. Control Div., Colo. Dep. of Public Health and Environ., Denver.

State of Wyoming (2011), Exceptional event demonstration package for the Environmental Protection Agency: South Pass, Wyoming Ozone Standard Exceedances on February 27–28, March 6–7, and March 10–13, 2009, report, Dep. of Environ. Qual., Cheyenne, Wyo.

Stevenson, D. S., et al. (2006), Multimodel ensemble simulations of present-day and near-future tropospheric ozone, *J. Geophys. Res.*, *111*, D08301, doi:10.1029/2005JD006338.

Stohl, A., and T. Trickl (1999), A textbook example of long-range transport: Simultaneous observation of ozone maxima of stratospheric and North American origin in the free troposphere over Europe, *J. Geophys. Res.*, *104*, 30,445–30,462, doi:10.1029/1999JD900803.

Stohl, A., et al. (2003), Stratosphere-troposphere exchange: A review, and what we have learned from STACCATO, *J. Geophys. Res.*, *108*(D12), 8516, doi:10.1029/2002JD002490.

Susskind, J., C. D. Barnet, and J. M. Blaisdell (2003), Retrieval of atmospheric and surface parameters from AIRS/AMSU/HSB data in the presence of clouds, *IEEE Trans. Geosci. Remote Sens.*, *41*, 390–409, doi:10.1109/TGRS.2002.808236.

Tarasick, D. W., et al. (2007), Comparison of Canadian air quality forecast models with tropospheric ozone profile measurements above mid-latitude North America during the IONS/ICARTT campaign: Evidence for stratospheric input, *J. Geophys. Res.*, *112*, D12S22, doi:10.1029/2006JD007782.

Terao, Y., J. A. Logan, A. R. Douglass, and R. S. Stolarski (2008), Contribution of stratospheric ozone to the interannual variability of tropospheric ozone in the northern extratropics, *J. Geophys. Res.*, *113*, D18309, doi:10.1029/2008JD009854.

Thompson, A. M., et al. (2007), Intercontinental Chemical Transport Experiment Ozonesonde Network Study (IONS) 2004: 2. Tropospheric ozone budgets and variability over northeastern North America, *J. Geophys. Res.*, *112*, D12S13, doi:10.1029/2006JD007670.

U.S. Environmental Protection Agency (U.S. EPA) (2006), Air quality criteria for ozone and related photochemical oxidants (2006 final), *EPA/600/R-05/004aF-cF*, U.S. Environ. Prot. Agency, Washington, D. C.

U.S. Environmental Protection Agency (U.S. EPA) (2007), Treatment of data influenced by exceptional events, *Fed. Regist.*, *72*(55), 13,560–13,581.

U.S. Environmental Protection Agency (U.S. EPA) (2010), National ambient air quality standards for ozone, *Fed. Regist.*, *75*(11), 2938–3052.

van Noije, T., H. Eskes, M. van Weele, and P. van Velthoven (2004), Implications of the enhanced Brewer-Dobson circulation in European Centre for Medium-Range Weather Forecasts reanalysis ERA-40 for the stratosphere-troposphere exchange of ozone in global chemistry transport models, *J. Geophys. Res.*, *109*, D19308, doi:10.1029/2004JD004586.

Whiteman, C. D., X. Bian, and S. Zhong (1997), Low-level jet climatology from enhanced rawinsonde observations at a site in the Southern Great Plains, *J. Appl. Meteorol.*, *36*, 1363–1376, doi:10.1175/1520-0450(1997)036<1363:LLJCFE>2.0.CO;2.

Wild, O., X. Zhu, and M. Prather (2000), Fast-J: Accurate simulation of in- and below-cloud photolysis in tropospheric chemical models, *J. Atmos. Chem.*, *37*(3), 245–282, doi:10.1023/A:1006415919030.

Wild, O., et al. (2007), Modeling the global tropospheric ozone budget: Exploring the variability in current models, *Atmos. Chem. Phys.*, *7*, 2643–2660, doi:10.5194/acp-7-2643-2007.

Wimmers, A. J., and J. L. Moody (2001), A fixed-layer estimation of upper tropospheric specific humidity from the GOES water vapor channel: Parameterization and validation of the altered brightness temperature product, *J. Geophys. Res.*, *106*(D15), 17,115–17,132, doi:10.1029/2000JD900713.

Wimmers, A. J., J. L. Moody, E. V. Browell, J. W. Hair, W. B. Grant, C. F. Butler, M. A. Fenn, C. C. Schmidt, J. Li, and B. A. Ridley (2003), Signatures of tropopause folding in satellite imagery, *J. Geophys. Res.*, *108*(D4), 8360, doi:10.1029/2001JD001358.

World Health Organization (2005), WHO air quality guidelines global update, report on a working group meeting, Bonn, Germany, 18–20 October, 2005, *Rep. E87950*, 25 pp., Geneva, Switzerland.

Zeng, G., O. Morgenstern, P. Braesicke, and J. A. Pyle (2010), Impact of stratospheric ozone recovery on tropospheric ozone and its budget, *Geophys. Res. Lett.*, *37*, L09805, doi:10.1029/2010GL042812.

Zhang, L., et al. (2011), Improved estimate of the policy-relevant background ozone in the United States using the GEOS-Chem global model with $1/2^\circ \times 2/3^\circ$ horizontal resolution over North America, *Atmos. Environ.*, *45*(37), 6769–6776, doi:10.1016/j.atmosenv.2011.07.054.